



HAL
open science

Adaptive RISE Feedback Control for Robotized Machining With PKMs: Design and Real-Time Experiments

Jonatan Martin Escorcia-Hernandez, Ahmed Chemori, Hipolito Aguilar-Sierra

► **To cite this version:**

Jonatan Martin Escorcia-Hernandez, Ahmed Chemori, Hipolito Aguilar-Sierra. Adaptive RISE Feedback Control for Robotized Machining With PKMs: Design and Real-Time Experiments. IEEE Transactions on Control Systems Technology, 2023, 31 (1), pp.39-54. 10.1109/TCST.2022.3169015 . lirmm-03664459

HAL Id: lirmm-03664459

<https://hal-lirmm.ccsd.cnrs.fr/lirmm-03664459>

Submitted on 11 May 2022

HAL is a multi-disciplinary open access archive for the deposit and dissemination of scientific research documents, whether they are published or not. The documents may come from teaching and research institutions in France or abroad, or from public or private research centers.

L'archive ouverte pluridisciplinaire **HAL**, est destinée au dépôt et à la diffusion de documents scientifiques de niveau recherche, publiés ou non, émanant des établissements d'enseignement et de recherche français ou étrangers, des laboratoires publics ou privés.

Adaptive RISE Feedback Control for Robotized Machining with PKMs: Design and Real-Time Experiments

Jonatan Martín Escorcía-Hernández, Ahmed Chemori *Senior Member, IEEE*, Hipólito Aguilar-Sierra

Abstract—The development of high-precision tasks, such as machining, needs a positioning device for the cutting tool with the smallest possible error. Multiple design factors need to be considered to ensure a mechatronic device successfully performs such tasks. One of these factors may be attributed to the control scheme, which is responsible for controlling the position of the machine. In view of the importance of designing a good control scheme for a robotic system, in this paper, we propose a new extension of the robust integral sign of the error (RISE) for the positioning device a parallel kinematic machine (PKM). This extension consists in including a nominal feedforward term based on the inverse dynamic model of the robot and replacing the RISE fixed feedback gains with adaptive ones. The RISE part of the proposed controller ensures semi-global asymptotic stability. Moreover, it can accommodate sufficiently smooth bounded disturbances. The feedforward part cancels the nonlinearities of the system, improving the tracking performance of the controller. The adaptive feedback gains produce corrective actions when an increase in the tracking errors is due to the contact forces that occur during the machining process. A Lyapunov-based stability analysis is conducted to prove the semi-global asymptotic stability of the proposed control solution. To show its effectiveness real-time experiments are performed for two case studies; the first one is on a free motion trajectory, and the second on milling experiments under three different forward speeds on SPIDER4, a redundantly actuated PKM.

Index Terms—RISE Control, Adaptive control, Parallel Kinematic Manipulators, Machining task, Stability analysis.

I. INTRODUCTION

PARALLEL kinematic machines (PKMs) are robotic devices consisting of a fixed base and a moving platform connected by two or more link sets. Currently, the study of this type of systems has generated a major interest within the research community owing to the advantages they present compared to serial kinematic machines (SKMs). Some of these advantages include higher stiffness owing to the closed kinematic chains, higher acceleration capabilities, and improved load capacity than SKMs [1]. However, PKMs are also associated with complex nonlinear dynamic models, several uncertainties including unknown or time-varying parameters,

sensor noise, variations in the operative environment (payload variation and/or contact forces), and in some cases, the actuation redundancy problem [2], [3], [4]. Moreover, it has been reported that the effect of the nonlinearities commonly increases when the system is operated at high accelerations, causing undesirable mechanical vibrations [5],[6]. Despite the above problems, PKMs have been successfully integrated into various areas requiring high precision, such as remote surgery, three-dimensional (3D) printing, object handling, and machining [7]. Traditionally classical machining tools have been built with a serial structure, e.g., standard turning and milling machines. In this configuration, the moving axes are connected serially; therefore, so each moving axis supports the following moving axes. However, the drawback of this configuration is that the moving elements of the machine have to be sufficiently heavy to provide appropriate stiffness to control the bending movements [8]. Unlike SKMs, machine tools based on PKMs present significant advantages in their mechanical structure, such as improved stiffness owing to the closed-loop mechanism design, lower moving masses and inertias, and potentially better accuracy [9]. The first machine tool prototype using a parallel structure mechanism was patented in 1995; it was named Variax [10]. This PKM was inspired by the six-degree of freedom (DOF) Gough–Stewart platform. Based on the design of this prototype, the machine tools of various devices with parallel structures have been developed over time, with Tricept [11], Octahedral-Hexapod [12], and Hexa Toyoda [13] as some of the most relevant examples of this category.

To fully utilize of the benefits offered by the closed-loop kinematic configuration of PKMs, one should design and implement an adequate control scheme for the positioning of the manipulator tool. This is highly important because to perform machining tasks, it is necessary to ensure precise trajectory tracking despite the problems caused by contact forces and abrupt forward speed changes. In the literature, various advanced control solutions have been reported to deal with the problem of motion control of PKMs. These control schemes can be categorized as adaptive control, robust control, or their combination [14]. Considering some recent schemes, in [15], an extended \mathcal{L}_1 adaptive controller was designed and implemented on a four-DOF redundantly actuated (RA)-PKM called ARROW, for milling applications [16]. This proposed approach consists of adding an adaptive feedforward model-based term to the original \mathcal{L}_1 adaptive controller. This modification notably enhanced the performance of ARROW

Manuscript received February 25, 2021; revised July 99, 9999.

The authors acknowledge The Mexican Council of Science and Technology (CONACYT), Mexico, for the Ph.D. scholarship of the first author. (*Corresponding Author: Ahmed Chemori*).

J. M. Escorcía-Hernández, is with Universidad Politécnica de Tulancingo, Calle Ingenierías No. 100 C.P. 43629, Tulancingo Hidalgo, México (e-mail: jonatan.escorcía@upt.edu.mx).

A. Chemori is with LIRMM, University of Montpellier, CNRS, Montpellier, France (e-mail: Ahmed.Chemori@lirmm.fr).

H. Aguilar-Sierra is with Facultad de Ingeniería. Universidad La Salle México, Benjamin Franklin No. 45, C.P. 06140, Ciudad de México, México (e-mail: hipolito.aguilar@lasalle.mx).

compared to that of the standard \mathcal{L}_1 adaptive controller, resulting in an approximately 80% improvement in the root mean square error (RMSE) of the tracking error. In [17], a new terminal sliding mode (TSM) controller was developed for PKMs; this controller incorporates an adaptive loop to estimate the dynamic parameters of the manipulator on-line, improving its dynamic capabilities. This motion control solution was validated by real-time experiments on a four-DOF PKM, Veloce, and the results showed that it outperformed the regular TSM. In [18], a desired compensation adaptive law (DCAL) controller with nonlinear feedback gains was developed and validated by real-time experiments on an RA-PKM, DUAL-V, designed for laser cutting purposes. The performance of this controller was compared to the original DCAL, showing a significant reduction in the tracking errors. In addition to these examples, in the last two decades, the use of robust integral sign of the error (RISE) controllers has become highly well-known for the motion control of robotic systems, including PKMs. The success of this non-model-based control scheme is owing to its capability to ensure semi-global asymptotic tracking under poorly or uncertain knowledge of the dynamics of complex nonlinear systems. RISE control includes a discontinuous nonlinear term providing the controller robustness to compensate the poorly known nonlinearities, considering that they are bounded and second-order differentiable. Moreover, RISE control is suitable to be extended with different feedforward compensating terms. This control scheme has been commonly used in control of PKMs; some relevant examples are mentioned below. Bennehar et al. proposed and implemented a RISE-based adaptive feedforward control [19]. The proposed adaptive feedforward term is formulated in a regressor matrix form to estimate the unknown dynamic parameters of a three-DOF delta PKM online. Saied et al. designed and validated a RISE control with nonlinear feedback gains for PKMs [20], demonstrating that the tracking error could be significantly reduced with the incorporation of time-varying gains in the control loop. In addition, in [21] RISE feedback control was complemented with neural networks where a B-spline neural network was employed to estimate the dynamics of a PKM online to incorporate it as a feedforward compensation term in the control law. Furthermore, in previous study of the authors [22], a RISE controller with nominal feedforward was applied to an RA-PKM, SPIDER4, which was designed to perform machining operations. This controller was used to validate the inverse dynamic model (IDM) of SPIDER4 by including it as a feedforward compensation term in the control law. The achieved performance was approximately 24% better, in terms of the Cartesian RMSE, than that of the standard RISE controller, demonstrating the need for an IDM of the robot. The use of a simplified IDM in this study can be justified as compromise between complexity and quality. Implementing a complete IDM would require a high computational burden, resulting in real-time issues, and thereby deteriorating the overall performance of the system.

Considering the need for high precision in applications such as machining, in this study, we establish a new RISE feedforward controller with adaptive feedback gains. This research aims at improving the trajectory tracking performance

of PKMs, which are designed for machining applications, such as milling or drilling, using a new control design. The adaptive feedback gains of the proposed control solution produce corrective actions when the tracking errors are considerably increased by contact forces involved in the machining process. These gains are adjusted according to a criterion based on the values of the joint tracking errors. It is worth mentioning that, the main difference between this study and the contribution of [20] lies in nature of the control schemes. In [20] the control solution uses nonlinear time-varying gains, whose variation is based on predefined fixed nonlinear functions. However, the proposed scheme in the present paper is based on adaptive feedback gains, whose variation is governed by adaptation laws. Furthermore, beyond the different kinematics as well as the target application, a nominal feedforward is used in the present study to improve the tracking performance.

The remainder of this paper is organized as follows: In Section 2, we introduce SPIDER4, an RA-PKM, describing its inverse kinematic model (IKM) and IDM. In Section 3, the proposed control solution is introduced, including the Lyapunov stability analysis of the resulting closed-loop system. Section 4 presents the obtained real-time experiments to validate the proposed control strategy. Finally, the general conclusion and the future study perspectives are addressed in Section 5.

II. DESCRIPTION AND MODELING OF SPIDER4 RA-PKM

SPIDER4 is an RA-PKM with five DOFs (3T–2R), designed to perform machining operations, such as drilling or milling, on resin materials. SPIDER4 is formed of two independent mechanisms: (i) the first one is a parallel mechanism inspired by the delta parallel architecture, which is responsible for performing the translational movements of the machine, (ii) the second is a serial wrist mechanism, which orients the spindle cutting tool in space. The overall dimensions of the machine are 4.6 m in length, 2.5 m in width, and 2.4 m in height. This parallel-machine tool was designed and manufactured in a collaboration between The Laboratoire d'Informatique, de Robotique et de Microélectronique de Montpellier (LIRMM), and the Tecnia company. Fig. 1-(a) shows a general overview of SPIDER4, and Fig. 1-(b) illustrates its main components. The parallel positioning device of SPIDER4 is composed of four kinematic chains connecting the fixed base to the traveling plate. Each kinematic chain includes a rear arm and a forearm, which is constituted by two parallel bars. Each kinematic chain is formed of one motor connected to its rear arm through a rotational joint; the rear arm, in turn, is joined to the forearm of the chain using universal joints; finally, the forearm is connected to the traveling plate through a universal joint. The wrist mechanism is located over the traveling plate; it is formed by two actuators and their coupling parts, supporting and orienting the spindle motor.

A. Inverse kinematic model

Following the description of the mechanism of SPIDER4, here the development of its IKM is presented, which consists of finding the generalized coordinates vector, $\mathbf{Q} =$

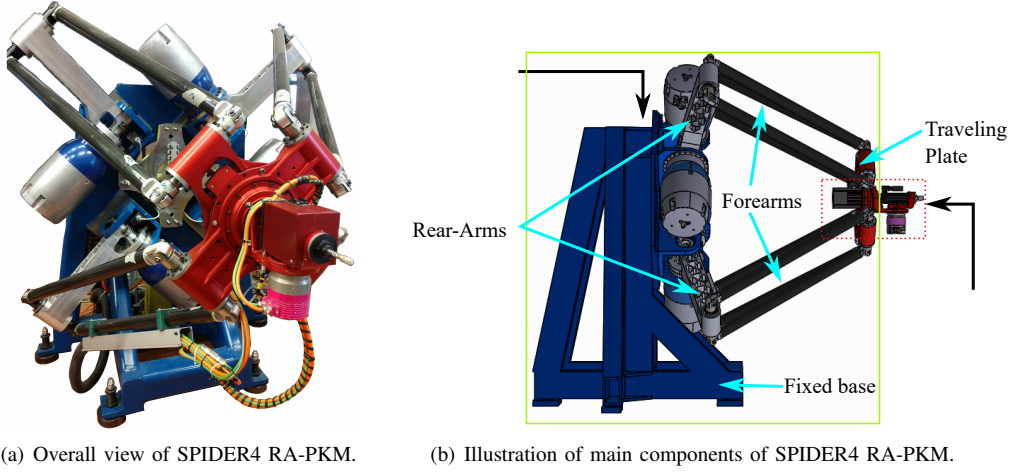


Fig. 1. Overview of SPIDER4 redundantly actuated parallel kinematic manipulator (RA-PKM) and its main components.

$[q_1 \ q_2 \ q_3 \ q_4 \ \phi \ \psi]^T \in \mathbb{R}^{6 \times 1}$, given the spindle position in the fixed reference frame, $O - x_o, y_o, z_o$, which is expressed as ${}^o\mathbf{S}_S = [x \ y \ z \ \phi \ \psi]^T \in \mathbb{R}^{5 \times 1}$. It is worth mentioning that variables ϕ and ψ are identical for the operational and joint spaces. However, because the proposed control scheme only involves the parallel structure of the delta-like positioning device of SPIDER4, the following position vector for the traveling plate needs to be defined: ${}^o\mathbf{N}_N = [x_n \ y_n \ z_n]^T \in \mathbb{R}^{3 \times 1}$, to compute the joint coordinates of the parallel structure $\mathbf{q} = [q_1 \ q_2 \ q_3 \ q_4]^T \in \mathbb{R}^{4 \times 1}$. As presented in [22], ${}^o\mathbf{N}_N$ is computed by a series of transformations involving the variables of the vector, ${}^o\mathbf{S}_S$, and the offset distances, A_{offset} and S_{offset} , illustrated in Fig. 2. The IKM solution for SPIDER4 is expressed as follows:

$$q_i = 2 \arctan \left(\frac{-D_i \pm \sqrt{\Delta_i}}{F_i - E_i} \right) \quad (1)$$

Above $\Delta_i = D_i^2 + E_i^2 - F_i^2$. Because ϕ and ψ are considered known for the IKM analysis, we can conclude that the IKM solutions for \mathbf{q} and \mathbf{Q} are obtained.

$D_i = 2L_i(({}^o\mathbf{C}_i - {}^o\mathbf{A}_i) \cdot \mathbf{z}_o)$, $E_i = 2L_i(({}^o\mathbf{C}_i - {}^o\mathbf{A}_i) \cdot {}^i\mathbf{x}_i)$, $F_i = l_i^2 - L_i^2 - \|{}^o\mathbf{C}_i - {}^o\mathbf{A}_i\|^2$, and $\mathbf{z}_o = [0 \ 0 \ 1]^T$. For more details of the methodology to obtain the IKM, the reader may referred to [22], [23], [24].

B. Inverse dynamic model of delta-like positioning device

This section briefly describes the IDM of the delta-like positioning device SPIDER4, considering the masses of the wrist elements. Obtaining a precise and complete IDM for PKMs has frequently been a complex task owing to the existence of coupling dynamics and the number of elements involved in the mechanism [25]. Moreover, a complete IDM may be unsuitable for real-time implementation owing to its high demand for computing resources to solve complex mathematical expressions, such as the pseudo-inverse of several non-square Jacobian matrices. Therefore, deriving a simplified IDM is an interesting solution for the real-time implementation of model-based ones, which may have a better performance than non-model-based controllers. For the development of the

IDM of the delta-like positioning device of SPIDER4, in this study, the simplification hypotheses for delta-like manipulators presented in [26] is considered. It is worth mentioning that these hypotheses also have been considered in previous studies [27], [28], [23]. The considered modeling simplifications are as follows:

- **Simplification hypothesis 1:** The dry and viscous frictions of the active and passive joints of SPIDER4 are neglected. This hypothesis is considered because our proposed control solution can compensate the unmodeled dynamics effects.
- **Simplification hypothesis 2:** The rotational inertia of the forearms is neglected, and its mass is divided into two equivalent parts; the first one is added to the rear arm mass, whereas the second is integrated to the traveling plate mass. This hypothesis is justified if the forearm mass is smaller than those of the rear arm and the traveling plate, as it occurs in the case of SPIDER4.

The IDM establishes the actuators input torque $\Gamma \in \mathbb{R}^{4 \times 1}$, as a function of (i) the torques produced by the traveling plate $\Gamma_{na} \in \mathbb{R}^{4 \times 1}$, (ii) the torques produced by the inertia of the actuators located at the fixed base $\Gamma_{act} \in \mathbb{R}^{4 \times 1}$, and (iii) the torques produced by the set of rear arm-forearm $\Gamma_{rfa} \in \mathbb{R}^{4 \times 1}$. The mathematical equation is denoted as follows:

$$\Gamma = \Gamma_{na} + \Gamma_{rfa} + \Gamma_{act} \quad (2)$$

To determine the torques acting on the traveling plate, it is necessary first to compute the inertial and gravity forces acting on it. To this end, we apply the Newton-Euler formulation. Subsequently, using the pseudoinverse Jacobian matrix we can map from the linear forces to the torques acting on the traveling plate, leading to the following equation:

$$\Gamma_{na} = \mathbf{H}^T \mathbf{M}_p ({}^o\ddot{\mathbf{N}}_N + \mathbf{g}) \quad (3)$$

where $\mathbf{H} \in \mathbb{R}^{3 \times 4}$ is the non-square pseudoinverse Jacobian matrix, $\mathbf{M}_p \in \mathbb{R}^{4 \times 4}$ is a diagonal mass matrix including the half masses of the forearms and the masses of the actuators located on the traveling plate, $\mathbf{g} \in \mathbb{R}^{3 \times 1}$ is the gravity vector expressed by $\mathbf{g} = [0 \ g \ 0]^T$ with $g = 9.81 \text{ m/s}^2$, and

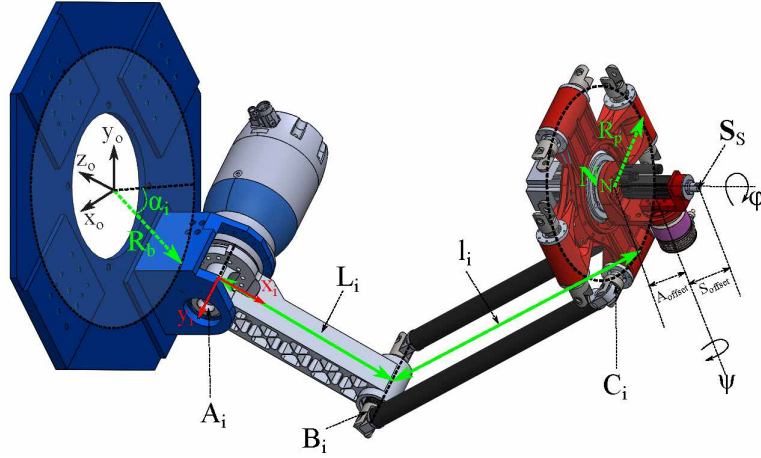


Fig. 2. Illustration of one kinematic chain of SPIDER4 RA-PKM.

${}^o\ddot{\mathbf{N}}_N \in \mathbb{R}^{3 \times 1}$ is the traveling plate acceleration vector. The matrix, $\mathbf{M}_p \in \mathbb{R}^{3 \times 3}$, is a diagonal matrix whose elements are as follows:

$$\mathbf{M}_p = m_{na} + m_{namotors} + 4 \frac{m_{fa}}{2} \quad \forall i = 1, \dots, 4 \quad (4)$$

where m_{na} represents the mass of the traveling plate, m_{fa} is the forearm mass composed of the mass of the two parallelogram bars, and $m_{namotors} = m_\phi + m_\psi + m_s$, is the masses of the three motors located at the traveling plate, including their coupling parts.

According to [22], the torques produced by the set of rear arm–forearm are related to the inertial and gravity forces as follows

$$\mathbf{\Gamma}_{rfa} = \mathbf{I}_{rfa} \ddot{\mathbf{q}} + g \mathbf{M}_{rfa} \cos(\mathbf{q}) \quad (5)$$

where $\mathbf{I}_{rfa} \in \mathbb{R}^{4 \times 4}$ is a diagonal matrix whose elements are formed by $I_{arm} + \frac{L^2 m_{fa}}{2}$, where I_{arm} and L are the inertia of one rear arm and its length, respectively. The term, $\cos(\mathbf{q}) \in \mathbb{R}^{4 \times 1}$, represents a vector of cosines as a function of each joint position of the actuators located at the fixed base, and $\mathbf{M}_{rfa} \in \mathbb{R}^{4 \times 4}$ is a diagonal matrix whose elements are as follows:

$$m_{rfa} = (m_{ra} L_c + \frac{m_{fa} L}{2}) \sin(\alpha_i) \quad \forall i = 1, \dots, 4 \quad (6)$$

Above m_{ra} is the mass of one rear arm, and L_c is the distance between its rotational axis and its center of mass. The components of (5) show the implication of the second hypothesis simplification, which involves consideration of the half masses of the forearms. Moreover, the term, $\sin(\alpha_i)$, represents the fixed orientation of each kinematic chains, i.e., the traveling plate cannot rotate.

Finally, the produced torques related to the inertia of the actuators are expressed in the following form:

$$\mathbf{\Gamma}_{act} = \mathbf{I}_{act} \ddot{\mathbf{q}} \quad (7)$$

where $\mathbf{I}_{act} \in \mathbb{R}^{4 \times 4}$ is a square diagonal matrix containing the inertia values of each motor placed over the fixed base. Equation (2) represents the IDM as a function of the joint and Cartesian space variables. Therefore, to rewrite it only

as a function of the joint variables, one should consider the following kinematic relationship based on the pseudoinverse Jacobian matrix:

$${}^o\ddot{\mathbf{N}}_N = \mathbf{H} \ddot{\mathbf{q}} + \dot{\mathbf{H}} \dot{\mathbf{q}} \quad (8)$$

By substituting (3), (5), and (7) in (2), using (8), and rearranging terms, we establish the IDM for the delta-like positioning device of SPIDER4 as follows:

$$\mathbf{M}(\mathbf{q}) \ddot{\mathbf{q}} + \mathbf{C}(\mathbf{q}, \dot{\mathbf{q}}) \dot{\mathbf{q}} + \mathbf{G}(\mathbf{q}) + \mathbf{f}(\mathbf{q}, \dot{\mathbf{q}}) = \mathbf{\Gamma} \quad (9)$$

where

- $\mathbf{M}(\mathbf{q}) = \mathbf{I}_{act} + \mathbf{I}_{rfa} + \mathbf{H}^T \mathbf{M}_p \mathbf{H}$
- $\mathbf{C}(\mathbf{q}, \dot{\mathbf{q}}) = \mathbf{H}^T \mathbf{M}_p \dot{\mathbf{H}}$
- $\mathbf{G}(\mathbf{q}) = \mathbf{H}^T \mathbf{M}_p \mathbf{G} + g \mathbf{M}_{rfa} \cos(\mathbf{q})$
- $\mathbf{f}(\mathbf{q}, \dot{\mathbf{q}})$ is a vector of the friction effects.

The kinematic and dynamic parameters of SPIDER4 are summarized in Table I. It is worth mentioning that the dynamic parameters as the masses of the rear arms, forearms, traveling plate, coupling parts, and the rear arms inertia were calculated using the material assignment functionality of SolidWorks software. However, the other dynamic parameters — the inertia of the motors and their masses— are obtained from the datasheets of the manufacturers of the actuators.

For further details about the complete IDM of SPIDER4 as well as the formulation of its Jacobian matrices, the reader can refer to [22].

The following notable properties of the IDM are assumed to hold for the subsequent stability analysis:

Property 2.1: The mass matrix, $\mathbf{M}(\mathbf{q}) \in \mathbb{R}^{n \times n}$, is symmetric positive-definite satisfying the following inequality [29]:

$$\underline{m} \|\zeta\|^2 \leq \zeta^T \mathbf{M}(\mathbf{q}) \zeta \leq \overline{m}(\mathbf{q}) \|\zeta\|^2, \quad \forall \zeta \in \mathbb{R}^n \quad (10)$$

where \underline{m} is a positive constant, $\overline{m}(\mathbf{q})$ is a positive non-decreasing function, and $\|\cdot\|$ represents the standard Euclidean norm.

Property 2.2: If \mathbf{q} and $\dot{\mathbf{q}}$ are measurable and bounded, then $\mathbf{C}(\mathbf{q}, \dot{\mathbf{q}})$ and $\mathbf{G}(\mathbf{q})$ are also bounded. Additionally, the first and second partial derivatives of the elements of $\mathbf{M}(\mathbf{q})$, $\mathbf{C}(\mathbf{q}, \dot{\mathbf{q}})$, and $\mathbf{G}(\mathbf{q})$ with respect to \mathbf{q} , and the first and second partial

TABLE I
SUMMARY OF KINEMATIC AND DYNAMIC PARAMETERS OF SPIDER4
RA-PKM.

Parameter	Description	Value
L	Rear arm length	0.535 m
l	Forearm length	1.100 m
R_b	Fixed base radius	0.4 m
R_p	Traveling plate radius	0.260 m
S_{offset}	Distance between ψ and ${}^o\mathbf{S}_S$	1.135 m
A_{offset}	Distance between ${}^o\mathbf{N}_N$ and ψ	0.198375 m
m_{na}	Traveling plate mass	22.76 kg
m_{ra}	Rear arm mass	17.6 kg
m_{fa}	Forearm mass	4.64 kg
I_{arm}	Rear arm inertia	1.69 kgm ²
I_{act}	Inertia of principal actuators	0.00223 kgm ²
m_s	Mass of spindle motor	3.2 kg
m_ψ	ψ motor mass	5.1 kg
m_ϕ	ϕ motor mass	11.2 kg

derivatives of the elements of $\mathbf{C}(\mathbf{q}, \dot{\mathbf{q}})$ and $\mathbf{f}(\dot{\mathbf{q}})$ with respect to $\dot{\mathbf{q}}$ exist and are also bounded.

Assumption 2.1: The desired trajectory, \mathbf{q}_d , is continuously differentiable with respect to time until the $(n+2)$ derivative.

III. PROPOSED CONTROL SCHEME: RISE FEEDFORWARD CONTROLLER WITH ADAPTIVE FEEDBACK GAINS

In this section, we address the main control contribution of the present study: a RISE feedforward controller with adaptive feedback gains. The nominal feedforward term includes the described IDM of the delta-like positioning device of SPIDER4 evaluated with the desired joint trajectories and their time derivatives. RISE is a robust feedback control strategy developed for uncertain nonlinear systems integrating a unique integral signum term that can ensure semi-global asymptotic stability in the presence of general uncertain disturbances [30]. This feature is of high importance when the dynamic parameters of the system to be controlled are fully or partially unknown. The model-based feedforward term partially cancels some nonlinearities of the system, reducing the tracking errors. As mentioned in the introduction, the adaptive gains of the proposed control solution produce further corrective actions when the tracking errors are considerably increased by the contact forces involved in the machining process for instance. Therefore, before presenting the mathematical formulation of our proposed control strategy, the definitions of various tracking errors are introduced. The first one is the tracking error in the joint space, $\mathbf{e}_1(t) \in \mathbb{R}^n$, which is defined as

$$\mathbf{e}_1(t) = \mathbf{q}_d(t) - \mathbf{q}(t) \quad (11)$$

where $\mathbf{q}_d(t) \in \mathbb{R}^n$ represents the vector of the desired trajectories in the joint space and n represents the number of actuators involved in the analysis, i.e. $n = 4$. The following filtered tracking errors are useful for the subsequent Lyapunov-based stability analysis [31]:

$$\mathbf{e}_2(t) = \dot{\mathbf{e}}_1(t) + \Lambda_1 \mathbf{e}_1(t) \quad (12)$$

$$\mathbf{r}(t) = \dot{\mathbf{e}}_2(t) + \Lambda_2(t) \mathbf{e}_2(t) \quad (13)$$

where $\Lambda_1 \in \mathbb{R}^{n \times n}$ is a positive-definite diagonal gain matrix and $\Lambda_2(t) \in \mathbb{R}^{n \times n}$ is an adaptive gain matrix. Thus, the proposed control law can be expressed as follows

$$\Gamma(t) = \Gamma_{ARISE} + \Gamma_{FF} \quad (14)$$

where $\Gamma_{FF} \in \mathbb{R}^n$ corresponds to the nominal feedforward term described in (15), and $\Gamma_{ARISE} \in \mathbb{R}^n$ is the RISE controller with adaptive feedback gains, whose mathematical expression is provided in (16)

$$\Gamma_{FF} = \mathbf{M}(\mathbf{q}_d) \ddot{\mathbf{q}}_d + \mathbf{C}(\mathbf{q}_d, \dot{\mathbf{q}}_d) \dot{\mathbf{q}}_d + \mathbf{G}(\mathbf{q}_d) \quad (15)$$

$$\begin{aligned} \Gamma_{ARISE}(t) &= (\mathbf{K}_s(t) + \mathbf{I}) \mathbf{e}_2(t) - (\mathbf{K}_s(t) + \mathbf{I}) \mathbf{e}_2(0) \\ &+ \int_0^t [(\mathbf{K}_s(\tau) + \mathbf{I}) \Lambda_2(\tau) \mathbf{e}_2(\tau) + \beta \text{sgn}(\mathbf{e}_2(\tau))] d\tau \end{aligned} \quad (16)$$

In the $\Gamma_{ARISE}(t)$ control term, $\beta \in \mathbb{R}^{n \times n}$ is a positive-definite diagonal gain matrix used to increase the controller robustness, and $\mathbf{K}_s(t)$ and $\Lambda_2(t) \in \mathbb{R}^{n \times n}$ are the adaptive gain matrices whose adjustments are inspired from the adaptation algorithm presented in [32]. The adaptive rules for the gain matrices are as follows:

$$\mathbf{K}_s(t) = \bar{\mathbf{K}}_s |\boldsymbol{\eta}| + \mathbf{K}_2 \quad (17)$$

$$\Lambda_2(t) = \bar{\Lambda}_2 |\boldsymbol{\eta}| + \mathbf{K}_3 \quad (18)$$

$$\dot{\boldsymbol{\eta}} = \tanh(\mathbf{e}_2) - \boldsymbol{\eta} \quad (19)$$

where $\bar{\mathbf{K}}_s$ and $\bar{\Lambda}_2 \in \mathbb{R}^{n \times n}$ denote positive-definite constant diagonal matrices used in the adaptation process of the control feedback gains, and \mathbf{K}_2 and $\mathbf{K}_3 \in \mathbb{R}^{n \times n}$ are other positive-definite constant diagonal matrices that establish the minimum possible value for each adaptive feedback gain. $|\cdot|$ is the modulus vector function, and $\boldsymbol{\eta} \in \mathbb{R}^n$ is a nonlinear function depending on the combined tracking error, \mathbf{e}_2 , which is a function that combines both position and velocity errors.

Equation (19) represents the dynamics of the adaptive gains. In (19), a hyperbolic tangent function is used to produce an effect similar to the signum function, but without generating prominent discontinuities for a better smoothness. The modulus vector function in (18) is used to obtain only positive gain values. Since $\boldsymbol{\eta}$ is directly related to the \mathbf{e}_2 error, by modifying parameter Λ_1 , the amplitude of the signals of \mathbf{K}_s and Λ_2 will be affected. If Λ_1 is increased, \mathbf{K}_s and Λ_2 will increase, and if Λ_1 decreases, they will also decrease. Consequently, it is suggested to set Λ_1 to one value in the gain tuning and subsequently adjust the two other gains.

A. Closed-loop system formulation

In this section the IDM of the delta-like positioning device of SPIDER4 RA-PKM, as expressed in (9), is considered together with the equations defining the proposed control law in (16)-(19). To express the resulting closed-loop system by starting from an open-loop formulation, both sides of (13) are multiplied by $\mathbf{M}(\mathbf{q})$ and utilize (11) and (12), leading to the following expression:

$$\begin{aligned} \mathbf{M}(\mathbf{q}) \mathbf{r} &= \mathbf{C}(\mathbf{q}, \dot{\mathbf{q}}) \dot{\mathbf{q}} + \mathbf{G}(\mathbf{q}) + \mathbf{f}(\mathbf{q}, \dot{\mathbf{q}}) - \Gamma_{ARISE}(t) \\ &+ \mathbf{M}(\mathbf{q}) (\ddot{\mathbf{q}}_d + \Lambda_1 \dot{\mathbf{e}}_1 + \Lambda_2(t) \mathbf{e}_2(t)) - \Gamma_{FF}(t) \end{aligned} \quad (20)$$

For stability analysis purposes, the derivative of (20) with respect to time is computed, leading to the following expression:

$$\begin{aligned} \mathbf{M}(\mathbf{q})\dot{\mathbf{r}} = & -\dot{\mathbf{M}}(\mathbf{q})\mathbf{r} + \mathbf{C}(\mathbf{q}, \dot{\mathbf{q}})\ddot{\mathbf{q}} + \dot{\mathbf{C}}(\mathbf{q}, \dot{\mathbf{q}})\dot{\mathbf{q}} + \dot{\mathbf{G}}(\mathbf{q}) + \dot{\mathbf{f}}(\mathbf{q}, \dot{\mathbf{q}}) \\ & + \mathbf{M}(\mathbf{q})\ddot{\mathbf{q}}_d + \dot{\mathbf{M}}(\mathbf{q})\dot{\mathbf{q}}_d + \Lambda_1(\mathbf{M}(\mathbf{q})\ddot{\mathbf{e}}_1 + \dot{\mathbf{M}}(\mathbf{q})\dot{\mathbf{e}}_1) \\ & + \mathbf{M}(\mathbf{q})(\Lambda_2(t)\dot{\mathbf{e}}_2(t) + \dot{\Lambda}_2(t)\mathbf{e}_2(t)) \\ & + \dot{\mathbf{M}}(\mathbf{q})\Lambda_2(t)\mathbf{e}_2(t) - \dot{\Gamma}_{ARISE} - \dot{\Gamma}_{FF} \end{aligned} \quad (21)$$

where the time derivative of Γ_{ARISE} can be expressed as follows:

$$\begin{aligned} \dot{\Gamma}_{ARISE} = & (\mathbf{K}_s(t) + \mathbf{I})\dot{\mathbf{e}}_2(t) + [(\mathbf{K}_s(t) + \mathbf{I})\Lambda_2(t) \\ & + \dot{\mathbf{K}}_s(t)]\mathbf{e}_2(t) + \beta \text{sgn}(\mathbf{e}_2(t)) \end{aligned} \quad (22)$$

We can rewrite (21) in the following form:

$$\mathbf{M}(\mathbf{q})\dot{\mathbf{r}} = -\frac{1}{2}\dot{\mathbf{M}}(\mathbf{q})\mathbf{r} + \mathbf{N}(\mathbf{e}_1, \mathbf{e}_2, \mathbf{r}, t) - \mathbf{e}_2(t) - \dot{\Gamma}_{ARISE} - \dot{\Gamma}_{FF} \quad (23)$$

where the nonlinear term, $\mathbf{N}(\mathbf{e}_1, \mathbf{e}_2, \mathbf{r}, t) \in \mathbb{R}^n$, is expressed as follows:

$$\begin{aligned} \mathbf{N}(\mathbf{e}_1, \mathbf{e}_2, \mathbf{r}, t) = & \mathbf{C}(\mathbf{q}, \dot{\mathbf{q}})\ddot{\mathbf{q}} + \dot{\mathbf{C}}(\mathbf{q}, \dot{\mathbf{q}})\dot{\mathbf{q}} + \dot{\mathbf{G}}(\mathbf{q}) + \dot{\mathbf{f}}(\mathbf{q}, \dot{\mathbf{q}}) \\ & + \mathbf{M}(\mathbf{q})\ddot{\mathbf{q}}_d + \dot{\mathbf{M}}(\mathbf{q})\dot{\mathbf{q}}_d + \Lambda_1(\mathbf{M}(\mathbf{q})\ddot{\mathbf{e}}_1 + \dot{\mathbf{M}}(\mathbf{q})\dot{\mathbf{e}}_1) \\ & + \mathbf{M}(\mathbf{q})(\Lambda_2(t)\dot{\mathbf{e}}_2(t) + \dot{\Lambda}_2(t)\mathbf{e}_2(t)) + \dot{\mathbf{M}}(\mathbf{q})\Lambda_2(t)\mathbf{e}_2(t) \\ & + \mathbf{e}_2(t) - \frac{1}{2}\dot{\mathbf{M}}(\mathbf{q})\mathbf{r} \end{aligned} \quad (24)$$

Here, we define the auxiliary function, $\mathbf{N}_d(\mathbf{q}_d, \dot{\mathbf{q}}_d, \ddot{\mathbf{q}}_d, t) \in \mathbb{R}^n$, used to facilitate the subsequent stability analysis of the resulting closed-loop system.

$$\begin{aligned} \mathbf{N}_d(\mathbf{q}_d, \dot{\mathbf{q}}_d, \ddot{\mathbf{q}}_d, t) = & \mathbf{M}(\mathbf{q}_d)\ddot{\mathbf{q}}_d + \dot{\mathbf{M}}(\mathbf{q}_d)\dot{\mathbf{q}}_d + \mathbf{C}(\mathbf{q}_d, \dot{\mathbf{q}}_d)\ddot{\mathbf{q}}_d \\ & + \dot{\mathbf{C}}(\mathbf{q}_d, \dot{\mathbf{q}}_d)\dot{\mathbf{q}}_d + \dot{\mathbf{G}}(\mathbf{q}_d) + \dot{\mathbf{f}}(\mathbf{q}_d, \dot{\mathbf{q}}_d) \end{aligned} \quad (25)$$

Substituting (25) in (23) leads to the following:

$$\mathbf{M}(\mathbf{q})\dot{\mathbf{r}} = -\frac{1}{2}\dot{\mathbf{M}}(\mathbf{q})\mathbf{r} + \mathbf{N}_d + \tilde{\mathbf{N}} - \mathbf{e}_2(t) - \dot{\Gamma}_{ARISE} - \mathbf{N}_{FF} \quad (26)$$

where $\tilde{\mathbf{N}} = \mathbf{N} - \mathbf{N}_d$ and $\mathbf{N}_{FF} = \dot{\Gamma}_{FF}$. Considering the properties introduced in Section 2, we can deduce that \mathbf{N}_d and $\tilde{\mathbf{N}}$ exist and are bounded. The auxiliary vector, $\tilde{\mathbf{N}}$ can be upper bounded using the mean value theorem [33] as follows:

$$\|\tilde{\mathbf{N}}\| \leq \rho(\|\mathbf{z}\|)\|\mathbf{z}\| \quad (27)$$

where $\|\cdot\|$ represents the Euclidean norm and $\mathbf{z}(t) \in \mathbb{R}^{3n}$ is an error vector defined as

$$\mathbf{z}(t) = [\mathbf{e}_1 \quad \mathbf{e}_2 \quad \mathbf{r}]^T \quad (28)$$

We can infer the following properties in the bounded function, $\|\tilde{\mathbf{N}}\|$

Property 3.1: The bounded function, $\|\tilde{\mathbf{N}}\|$, is non-decreasing in $\|\mathbf{z}\|$.

1) *Bounds of adaptive gains:* Because nonlinear functions $\mathbf{K}_s(t)$ and $\Lambda_2(t)$ are continuously differentiable, they can be bounded in the following form:

$$\mathbf{K}_2 \leq \mathbf{K}_s(t) \leq \mathbf{K}_{sM} \quad (29)$$

$$\mathbf{K}_3 \leq \Lambda_2(t) \leq \Lambda_{2M} \quad (30)$$

where \mathbf{K}_{sM} and $\Lambda_{2M} \in \mathbb{R}^{n \times n}$ represent the maximum admissible values that $\mathbf{K}_s(t)$ and $\Lambda_2(t)$ may acquire. Moreover, it is assumed that \mathbf{K}_{sM} and Λ_{2M} exist but are unknown. \mathbf{K}_2 and $\mathbf{K}_3 \in \mathbb{R}^{n \times n}$ are positive-definite diagonal matrices whose elements denote the minimum possible values that $\mathbf{K}_s(t)$ and $\Lambda_2(t)$ can achieve. The values of \mathbf{K}_2 and \mathbf{K}_3 are determined in the tuning procedure of the controller.

2) *Stability analysis:* Before presenting the stability analysis of the closed-loop system with the proposed control solution, we introduce the below lemma, which can be considered as a modified version of Lemma 1 presented in [30].

Lemma 1: Let $\mathbf{L}(t) \in \mathbb{R}^n$ be an auxiliary function defined as:

$$\mathbf{L}(t) = \mathbf{r}(\mathbf{N}_d(t) - \mathbf{N}_{FF}(t) - \beta \text{sgn}(\mathbf{e}_2)) \quad (31)$$

If the controller gain, β , is chosen to satisfy the following inequality:

$$\begin{aligned} \beta > & \|\mathbf{N}_d(t)\|_{\mathcal{L}_\infty} - \|\mathbf{N}_{FF}(t)\|_{\mathcal{L}_\infty} \\ & + \frac{1}{\Lambda_{2M}} \left(\|\dot{\mathbf{N}}_d(t)\|_{\mathcal{L}_\infty} - \|\dot{\mathbf{N}}_{FF}(t)\|_{\mathcal{L}_\infty} \right) \end{aligned} \quad (32)$$

then

$$\int_0^t \mathbf{L}(\tau) d\tau \leq \zeta_b \quad (33)$$

where ζ_b is a positive constant defined as

$$\zeta_b = \beta \|\mathbf{e}_2(0)\| + \mathbf{e}_2(0)^T (\mathbf{N}_{FF}(0) - \mathbf{N}_d(0)) \quad (34)$$

Proof 1: The integral with respect to time of both sides of (31) leads to the following [31]:

$$\int_0^t \mathbf{L}(\tau) d\tau = \int_0^t \mathbf{r}(\tau) (\mathbf{N}_d(\tau) - \mathbf{N}_{FF}(\tau) - \beta \text{sgn}(\mathbf{e}_2(\tau))) d\tau \quad (35)$$

By substituting (13) into (35), we obtain

$$\begin{aligned} \int_0^t \mathbf{L}(\tau) d\tau = & \int_0^t \Lambda_2 \mathbf{e}_2(\tau)^T (\mathbf{N}_d(\tau) - \mathbf{N}_{FF}(\tau) - \beta \text{sgn}(\mathbf{e}_2(\tau))) d\tau \\ & + \int_0^t \frac{d\mathbf{e}_2(\tau)^T}{dt} \mathbf{N}_d(\tau) d\tau - \int_0^t \frac{d\mathbf{e}_2(\tau)^T}{d\tau} \mathbf{N}_{FF}(\tau) d\tau \\ & - \int_0^t \frac{d\mathbf{e}_2(\tau)^T}{d\tau} \beta \text{sgn}(\mathbf{e}_2(\tau)) d\tau \end{aligned} \quad (36)$$

Conducting integration by parts of the right-hand side of (36), the following is obtained:

$$\begin{aligned} \int_0^t \mathbf{L}(\tau) d\tau &= \int_0^t \Lambda_2 \mathbf{e}_2(\tau)^T (\mathbf{N}_d(\tau) - \mathbf{N}_{FF}(\tau)) d\tau \\ &- \int_0^t \frac{d\mathbf{e}_2(\tau)^T}{d\tau} \beta \text{sgn}[\mathbf{e}_2(\tau)] d\tau \\ &+ \mathbf{e}_2(\tau)^T \mathbf{N}_d|_0^t - \int_0^t \mathbf{e}_2(\tau) \frac{d\mathbf{N}_d(\tau)}{d\tau} - \mathbf{e}_2(\tau)^T \mathbf{N}_{FF}|_0^t \\ &+ \int_0^t \mathbf{e}_2(\tau) \frac{d\mathbf{N}_{FF}(\tau)}{d\tau} \end{aligned} \quad (37)$$

By rearranging the terms of (37), we obtain

$$\begin{aligned} \int_0^t \mathbf{L}(\tau) d\tau &= \int_0^t \Lambda_2 \mathbf{e}_2(\tau)^T (\mathbf{N}_d(\tau) - \mathbf{N}_{FF}(\tau)) \\ &+ \frac{1}{\Lambda_2} \left(\frac{d\mathbf{N}_{FF}(\tau)}{d\tau} \frac{d\mathbf{N}_d(\tau)}{d\tau} \right) - \beta \text{sgn}(\mathbf{e}_2(\tau)) \Big) d\tau \\ &+ \mathbf{e}_2^T(t) (\mathbf{N}_d(t) - \mathbf{N}_{FF}(t)) - \mathbf{e}_2^T(0) (\mathbf{N}_d(0) - \mathbf{N}_{FF}(0)) \\ &- \beta \|\mathbf{e}_2(t)\| + \beta \|\mathbf{e}_2(0)\| \end{aligned} \quad (38)$$

By upper bounding the right-hand side of (38), the following is obtained:

$$\begin{aligned} \int_0^t \mathbf{L}(\tau) d\tau &\leq \int_0^t \Lambda_2 \|\mathbf{e}_2(\tau)\| (\|\mathbf{N}_d(\tau)\| - \|\mathbf{N}_{FF}(\tau)\|) \\ &+ \frac{1}{\Lambda_2} \left(\left\| \frac{d\mathbf{N}_{FF}(\tau)}{d\tau} \right\| - \left\| \frac{d\mathbf{N}_d(\tau)}{d\tau} \right\| \right) - \beta \Big) d\tau \\ &+ \|\mathbf{e}_2(t)\| (\|\mathbf{N}_d(t)\| - \|\mathbf{N}_{FF}(t)\| - \beta) + \beta \|\mathbf{e}_2(0)\| \\ &+ \mathbf{e}_2^T(0) (\mathbf{N}_{FF}(0) - \mathbf{N}_d(0)) \end{aligned} \quad (39)$$

We can infer from (39) that if β is selected according to (32), then (33) is satisfied.

Theorem 1: The tracking error in the joint space, \mathbf{e}_1 , of the delta-like positioning device of SPIDER4, or any robotic system whose dynamics is governed by (9), under the control law in (14), converges semi-globally asymptotically to zero as long as time approaches infinity if the design parameters are selected such that

- i) $\Lambda_1 > \frac{1}{2}$
- ii) $\Lambda_{2M} > K_3$
- iii) $\beta > \|\mathbf{N}_d(t)\|_{\mathcal{L}^\infty} - \|\mathbf{N}_{FF}(t)\|_{\mathcal{L}^\infty}$
 $+ \frac{1}{\Lambda_{2M}} \left(\|\dot{\mathbf{N}}_d(t)\|_{\mathcal{L}^\infty} - \|\dot{\mathbf{N}}_{FF}(t)\|_{\mathcal{L}^\infty} \right)$

Proof 2: Let $\mathcal{D} \subset \mathbb{R}^{3n+1}$ be a domain containing

$$\mathbf{y}(t) = [\mathbf{z}^T(t) \quad \sqrt{\mathbf{P}(t)}]^T = \mathbf{0} \quad (40)$$

where $\mathbf{P}(t) \in \mathbb{R}^n$ is an auxiliary function defined as

$$\mathbf{P}(t) = \beta \|\mathbf{e}_2(0)\| - \mathbf{e}_2(0)^T (\mathbf{N}_{FF}(0) - \mathbf{N}_d(0)) - \int_0^t \mathbf{L}(\tau) d\tau \quad (41)$$

The time-derivative of (41) can be written as follows:

$$\dot{\mathbf{P}}(t) = -\mathbf{r}^T (\mathbf{N}_d(t) - \mathbf{N}_{FF}(t) - \beta \text{sgn}(\mathbf{e}_2)) = -\mathbf{L}(t) \quad (42)$$

Thus, we note that $\mathbf{P}(t) \geq 0, \forall t \geq 0$, considering (32) and (33).

Here, we define the Lyapunov candidate function, $\mathbf{V}(\mathbf{y}, t) : \mathcal{D} \times [0, \infty) \rightarrow \mathbb{R}$, as a continuously differentiable positive-definite function as follows

$$\mathbf{V}(\mathbf{y}, t) = \frac{1}{2} \mathbf{r}^T \mathbf{M}(\mathbf{q}) \mathbf{r} + \mathbf{e}_1^T \mathbf{e}_1 + \frac{1}{2} \mathbf{e}_2^T \mathbf{e}_2 + \mathbf{P} \quad (43)$$

Equation (43) can be bounded as follows:

$$\lambda_1 \|\mathbf{y}\|^2 \leq \mathbf{V}(\mathbf{y}, t) \leq \lambda_2 (\|\mathbf{y}\|) \|\mathbf{y}\|^2 \quad (44)$$

where

$$\lambda_1 = \frac{1}{2} \min\{1, \underline{m}\}, \quad \lambda_2(\|\mathbf{y}\|) = \max\{\frac{1}{2} \bar{m}(\|\mathbf{y}\|), 1\}$$

Because the gain matrices of the controller are diagonal-square, we can utilize only one of their elements when multiplying with vectors to simplify the stability analysis. Taking the time derivative of (43) and utilizing (42), (23), (22), (13), and (12), the following equation results:

$$\begin{aligned} \dot{\mathbf{V}}(\mathbf{y}, t) &= \mathbf{r}^T \dot{\mathbf{N}} - (K_s(t) + 1) \mathbf{r}^T \mathbf{r} - \dot{K}_s(t) \mathbf{r}^T \mathbf{e}_2 + 2\mathbf{e}_1^T \dot{\mathbf{e}}_2 \\ &- 2\Lambda_1 \mathbf{e}_1^T \mathbf{e}_1 - \Lambda_2(t) \mathbf{e}_2^T \mathbf{e}_2 \end{aligned} \quad (45)$$

where the terms $\mathbf{r}^T \mathbf{r}$, $\mathbf{e}_1^T \mathbf{e}_1$, $\mathbf{e}_2^T \mathbf{e}_2$, and $\mathbf{e}_2^T \mathbf{e}_1$ can be upper bounded as follows:

$$\begin{aligned} \mathbf{r}^T \mathbf{r} &\leq \|\mathbf{r}\|^2, \quad \mathbf{e}_1^T \mathbf{e}_1 \leq \|\mathbf{e}_1\|^2, \quad \mathbf{e}_2^T \mathbf{e}_2 \leq \|\mathbf{e}_2\|^2, \\ \mathbf{e}_2^T \mathbf{e}_1 &\leq \frac{1}{2} \|\mathbf{e}_1\|^2 + \frac{1}{2} \|\mathbf{e}_2\|^2 \end{aligned} \quad (46)$$

Considering the lower bounds of $\mathbf{K}_s(t)$ and $\Lambda_2(t)$ and the relationships in (46), (45) can be bounded as follows:

$$\begin{aligned} \dot{\mathbf{V}}(\mathbf{y}, t) &\leq \|\mathbf{r}\| \rho(\|\mathbf{z}\|) \|\mathbf{z}\| - (K_2 + 1) \|\mathbf{r}\|^2 \\ &- \frac{|K_{sdm}|}{2} \|\mathbf{r}\|^2 - \frac{|K_{sdm}|}{2} \|\mathbf{e}_2\|^2 + \|\mathbf{e}_1\|^2 + \|\mathbf{e}_2\|^2 \\ &- 2\Lambda_1 \|\mathbf{e}_1\|^2 - K_3 \|\mathbf{e}_2\|^2 \end{aligned} \quad (47)$$

where K_{sdm} denotes the lower bound of $\dot{\mathbf{K}}_s(t)$ as stated in [20]. The previous equation can be rewritten in the following form:

$$\dot{\mathbf{V}}(\mathbf{y}, t) \leq -\lambda_3 \|\mathbf{z}\|^2 - (K_2 \|\mathbf{r}\|^2 - \rho(\|\mathbf{z}\|) \|\mathbf{r}\| \|\mathbf{z}\|) \quad (48)$$

where, $\mathbf{z}(t) \in \mathbb{R}^{3n}$ represents the vector containing the different tracking errors of the system as expressed by (28), and $\lambda_3 = \min\{\eta_1, \eta_2, \eta_3\}$, where constants η_1 , η_2 , and η_3 are chosen as

$$\eta_1 = 2\Lambda_1 - 1, \quad \eta_2 = \frac{|K_{sdm}|}{2} + K_3 - 1, \quad \eta_3 = \frac{|K_{sdm}|}{2} + 1 \quad (49)$$

From (49), one can infer that Λ_1 must be chosen such that $\Lambda_1 > 1/2$. By completing the squares of the second and last terms of (48), the following expression is obtained:

$$\dot{\mathbf{V}}(\mathbf{y}, t) \leq -\lambda_3 \|\mathbf{z}\|^2 + \frac{\rho^2(\mathbf{z}) \|\mathbf{z}\|^2}{4K_2} = -c \|\mathbf{z}\|^2 \quad (50)$$

In (50), the term, $c \|\mathbf{z}\|^2$, denotes a continuous positive semi-definite function evolving in the following domain:

$$\mathcal{D} = \left\{ \mathbf{y} \leq \mathbb{R}^{3n+1} \mid \|\mathbf{y}\| \leq \rho^{-1} \left(2\sqrt{\lambda_3 K_2} \right) \right\} \quad (51)$$

We define \mathcal{S} as a subset of \mathcal{D} as follows:

$$\mathcal{S} = \left\{ \mathbf{y}(t) \in \mathcal{D} \mid c\|\mathbf{z}\|^2 < \lambda_3 \left(\rho^{-1} \left(2\sqrt{\lambda_3 K_2} \right) \right)^2 \right\} \quad (52)$$

According to [19], $c\|\mathbf{z}\|^2$ is consistently continuous in \mathcal{D} . Thus, based on theorem 8.4 of [34], we can conclude that

$$c\|\mathbf{z}\|^2 \rightarrow 0 \quad \text{as } t \rightarrow \infty, \quad \forall \mathbf{y}(0) \in \mathcal{S} \quad (53)$$

Therefore, based on the definition of $\mathbf{z}(t)$, we can deduce that

$$\|\mathbf{e}_1\| \rightarrow 0 \quad \text{as } t \rightarrow \infty, \quad \forall \mathbf{y}(0) \in \mathcal{S} \quad (54)$$

This concludes the stability proof of the proposed control solution.

B. Actuation redundancy issue in SPIDER4

There are various challenges associated with the control of PKMs. One of them lies in the actuation redundancy present in some parallel robots having more actuators than the degrees of freedom [35],[36]. This is the case for SPIDER4, which has five-DOFs (3T-2T), where the positioning device ensures the 3T DOFs using four actuators located at the fixed base. RA-PKMs have some advantages compared to their non-redundant counterparts, such as higher accuracy and improved stiffness. Furthermore, the actuation redundancy can also lead to singularity-free large workspaces. However, such a configuration may lead to the generation of internal forces, producing a pre-stress in the mechanism without operational motions, which can damage the mechanical structure of a robot. According to [3], internal forces can be caused by geometric uncertainties, and their effect may be amplified by decentralized control techniques. This decentralization may lead to uncoordinated control of the individual actuators of the robot because such control strategies do not consider kinematic constraints. To avoid such an issue, the use of a projection matrix can be considered, which is based on the pseudoinverse Jacobian matrix evaluated in terms of the desired variables, $\mathbf{H}(\mathbf{q}_d, {}^o\mathbf{N}_{Nd}) \in \mathbb{R}^{m \times n}$. The projection operator is expressed as [3]

$$\mathbf{R}_H = (\mathbf{H}^+)^T \mathbf{H}^T \quad (55)$$

The projection matrix, \mathbf{R}_H , eliminates the control inputs in the null-space of \mathbf{H}^T . This null-space projection was used to remove the controller effects that could produce antagonistic forces in the PKM. Hence, all control inputs applied to SPIDER4 have to be "regularized" using this projection matrix as follows:

$$\mathbf{\Gamma}^* = \mathbf{R}_H \mathbf{\Gamma} \quad (56)$$

where $\mathbf{\Gamma}$ denotes the torque vector generated by the proposed control law in (14). Fig. 3 illustrates the block diagram of the proposed controller for the delta-like positioning device of SPIDER4, including the projection operator.

IV. REAL-TIME EXPERIMENTAL RESULTS

To demonstrate the effectiveness of the proposed RISE feedforward control with adaptive feedback gains, we compare its performance in two case studies as follows:

- 1) *Case study 1: Nominal scenario.* In this case study, the performance of the proposed RISE feedforward with adaptive feedback gains is compared to those of a PID controller, and a PID feedforward controller. In this scenario, the controllers perform a free motion trajectory.
- 2) *Case study 2: Machining scenario.* In this case study, the performance of the proposed RISE feedforward with adaptive feedback gains is compared to those of a RISE feedforward controller and a standard RISE feedback controller. This case study is divided in three scenarios of the machining process: low, medium, and high-speed.

To simplify the notation, the proposed RISE feedforward with adaptive feedback gains is as denoted RISE FF AG, RISE feedforward as RISE FF, PID feedforward as PID FF, and the standard RISE control as only RISE.

A. Description of experimental setup

SPIDER4 uses different actuators to achieve linear motions of the parallel positioning device and the serial wrist holding the machining tool. Four WITTESTEIN TPMA110S-022M-6KB1-220H-W6 actuators are responsible for performing the movements along the axes x , y , and z . Each actuator includes a gearhead with a gear ratio of 1:22, a peak torque of 3100 Nm, and 189 rpm as the maximum rotation speed. These motors are equipped with multiturn absolute encoders to measure in real time the joint positions. Although the control scheme only uses the motors of the SPIDER4 parallel structure, it is worth mentioning the features of the traveling plate motors. On the traveling plate, three actuators perform independent angular motions ϕ and ψ as well as the movement of the spindle. The motor responsible for the movement along the ϕ axis is a STOBBER EZH501USVC4P097 motor; this actuator can generate a peak torque of 200 Nm. To perform the angular motion along the ψ axis, a HARMONIC DRIVE CHA-20A-30-H-M1024-B is used; this motor can provide a peak torque of 27 Nm. Finally, the B&R 8JSA24.E4080D000-0 is used for the actuation of the spindle machining tool. This motor can provide a torque of 1.41 Nm and a rotation speed of 8000 rpm. The joint velocities of SPIDER4 are not measured directly because the machine is not equipped with sensors to measure the joint velocities. Nevertheless, such velocities are calculated by numerical derivatives of the measurements of the joint positions with a sampling time of 0.4 ms. Fig. 4 shows the experimental setup of SPIDER4 in its work cell, including the tooling plate used to fix the material block to be machined. The architecture of each control scheme is created in Simulink software from MathWorks. The Simulink project includes the kinematic algorithms, Jacobian matrices, and control scheme for SPIDER4. However, all functionalities of SPIDER4, including the motion control, are programmed in a B&R Automation Studio project. Accordingly, a specific library called B&R Automation studio target for Simulink is used to convert the Simulink code into C code and transfer it to the B&R Automation Studio Project. The program is executed by a B&R Automation PC 910 with a programmed sampling time of 0.4 ms. The industrial PC sends and receives the control signals to the X20 system, which sends and

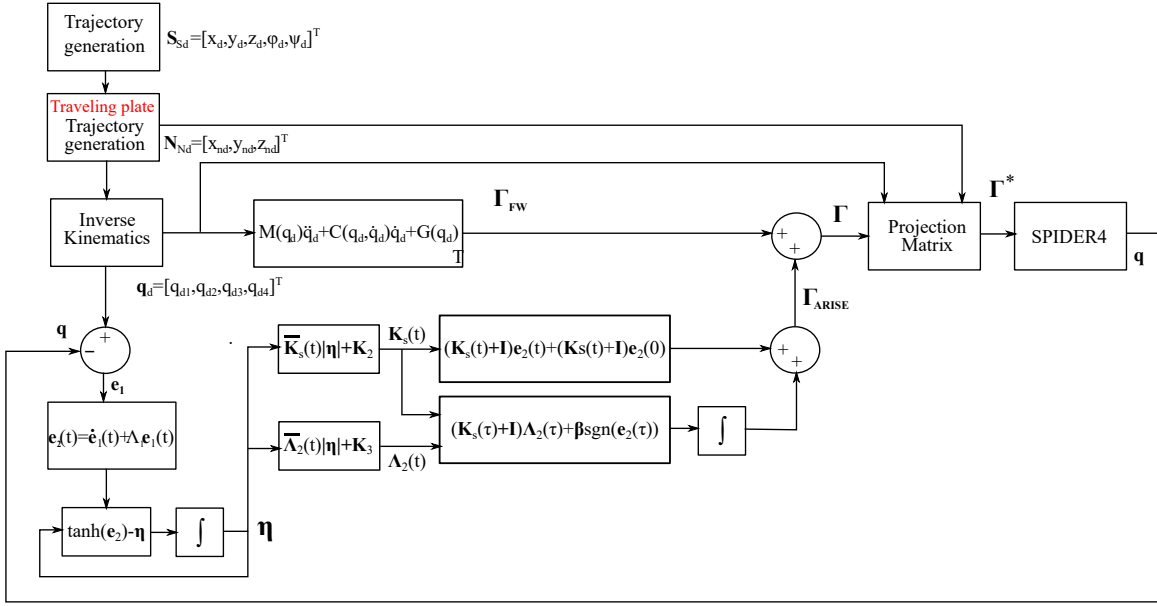


Fig. 3. Block diagram of the proposed control solution for SPIDER4 RA-PKM.

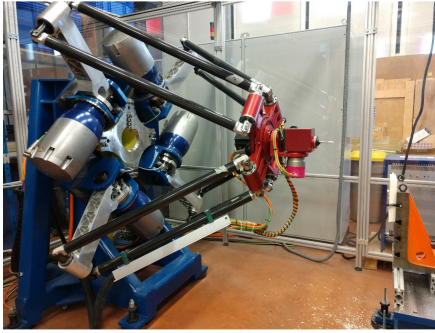


Fig. 4. Side view of experimental setup of SPIDER4 RA-PKM.

receives signals to the inverter modules called ACOPOS multi system, which produces the motion of each actuator. The SPIDER4 project is executed by a Graphic User Interface (GUI) developed by Tecnalía Company, programmed also in B&R Automation Studio.

B. Tuning gains procedure

The feedback gains of the controllers tested on SPIDER4 are tuned by a trial and error method, where particular focus should be paid to the existence of noise, which can be considerably amplified if the gains are not selected well, which may deteriorate the performance of the system. However, it is difficult for real-time experiments to realize gain tuning analytically when the dynamics is highly nonlinear, complex and the measurements are noisy. Consequently the best solution is the trial and error method until a good performance is achieved. For the proposed RISE FF AG controller, first, we set a sufficiently large value for Λ_1 ; subsequently, gains K_2 and K_3 are set as the minimum values that $\bar{K}_s(t)$ and $\bar{\Lambda}_2(t)$ could obtain, respectively. Gains \bar{K}_s and $\bar{\Lambda}_2$ are tuned according to the desired sensitivity to the changes in the

TABLE II
SUMMARY OF CONTROL DESIGN GAINS

PID/PID FF	RISE/RISE FF	RISE FF AG
$K_P = 160$	$\Lambda_1 = 110$	$\Lambda_1 = 110$
$K_D = 20$	$\Lambda_2 = 1$	$\bar{\Lambda}_2 = 3500$
$K_I = 80$	$K_s = 33$	$\bar{K}_s = 3500$
	$\beta = 0.5$	$\beta = 0.5$
		$K_2 = 33$
		$K_3 = 1$

tracking error in the joint space to increase the output values of $K_s(t)$ and $\Lambda_2(t)$. The value of gain β can increase the robustness of the controller. However, this value must be set very small at the beginning and gradually increased, to avoid the phenomenon of chattering. For PID/ PID FF controllers, we first set the K_P gain to be sufficiently large to produce motion in the robot while keeping the K_D and K_I gains as zero. Subsequently, we performed the K_D gain adjustment to decrease the oscillations, and finally, we adjusted the K_I gain value to reduce the transient state error.

It is worth mentioning that due to the existence of unknown/unmodelled phenomena such as friction in the real system, it is not recommended to tune the gains in a simulation procedure since the control design is based on a simplified dynamic model. The gains values of the proposed controllers implemented and validated in the experiments are summarized in Table II.

C. Reference trajectories generation

The B&R automation studio project of SPIDER4 incorporates a computer numerical control function, allowing define a desired trajectory using G-Code instructions.

1) *Case study 1:* The trajectory proposed for this scenario is shown in Fig. 5; it is worth mentioning that this trajectory can

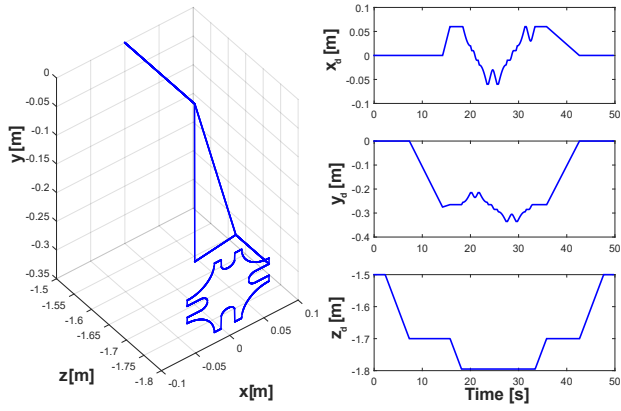


Fig. 5. Desired trajectory used for case study 1.

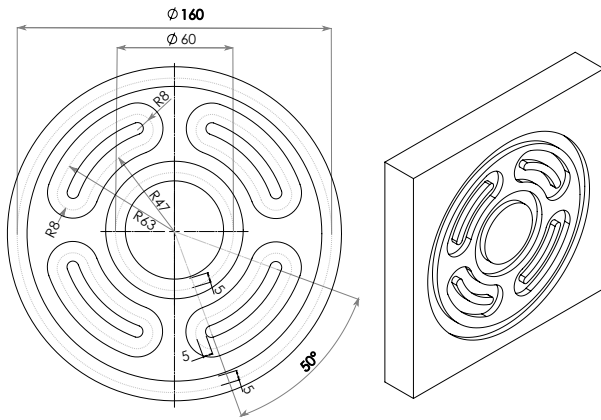


Fig. 6. Illustration of desired piece to be machined with its dimensions in mm and degrees.

be used for a milling task. However, in this case, the spindle is kept deactivated and we do not place the material to fabricate a part. The established forward speed for this experiment is $F=2400 \text{ mm/min}$. The left side of Fig. 5 depicts a 3D view of the desired path, whereas the right side of the figure illustrates the evolution of the trajectories for x , y , and z with respect to time.

2) *Case study 2:* The desired trajectory for this case study describes a milling machining process on a flat piece of styrofoam with a thickness of 1 in. The G-Code for this milling machining task was first simulated in WinUnisoft software from Alecop, to ensure safety of implementation on SPIDER4. The cutting depth established for the intended experiments was 5 mm, and the cutting speed established for the spindle, S , was 7000 rpm. One can modify the speed, S , from the G-Code; however, it is impossible to change it in real time with architecture and control. Fig. 7 illustrates the flat piece to be machined with its dimensions in millimeters. The machining trajectory generated by the G-Code is shown in 3D in Fig. 7. In the figure, the lines in red describe the part of the trajectory where the PKM is not cutting the material (free motion), whereas blue lines represent the sections of the trajectory where the spindle is cutting the piece (constrained motion).

To validate the effectiveness of the proposed control scheme,

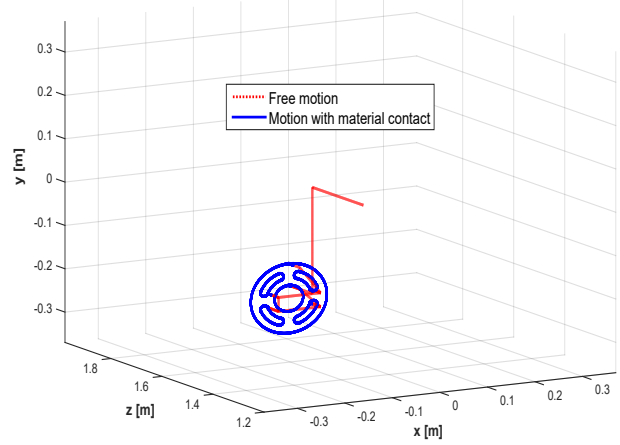


Fig. 7. Three-dimensional view of desired trajectory for intended machining task.

we executed the desired trajectory with the following three forward speeds (F):

- $F=1200 \text{ mm/min}$ (low speed)
- $F=2400 \text{ mm/min}$ (medium speed)
- $F=24000 \text{ mm/min}$ (high speed)

The desired trajectories in the Cartesian space (for x , y , and z) versus time for these forward speeds respectively are depicted in Fig. 8.

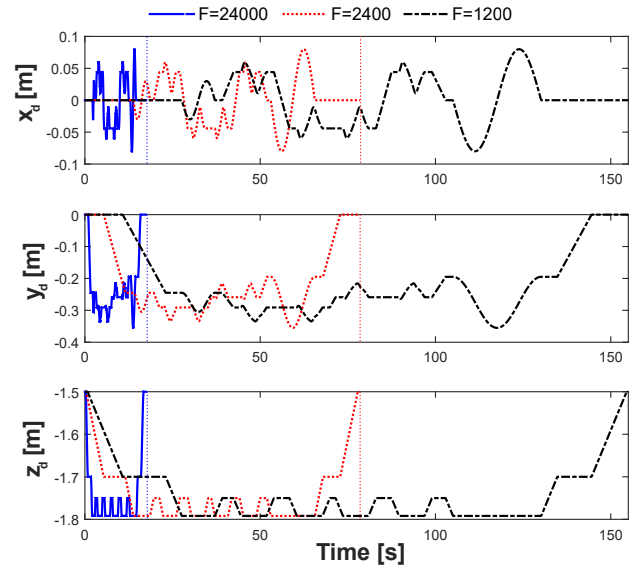


Fig. 8. Evolution of desired Cartesian trajectories versus time for different forward speeds F .

D. Performance evaluation criteria

We propose to use the RMSE, and the mean square error (MSE) formulas [37] to quantify the tracking performance of the control schemes. These formulas enable quantifying the degree of accuracy achieved by the tested controller numerically. The RMSE expressions for the SPIDER4 positioning device

TABLE III

PERFORMANCE COMPARISON OF CONTROLLERS USING RMSE AND MSE

Controller	RMSE	MSE
PID	0.0579	0.0848
PID FF	0.0570	0.0792
RISE FF AG	0.04721	0.0739

in the Cartesian ($RMSE_C$) and joint ($RMSE_J$) spaces are as follows:

$$RMSE_C = \sqrt{\frac{1}{N} \sum_{k=1}^N (e_{xn}^2(k) + e_{yn}^2(k) + e_{zn}^2(k))} \quad (57)$$

$$RMSE_J = \sqrt{\frac{1}{N} \sum_{k=1}^N (e_{11}^2(k) + e_{12}^2(k) + e_{13}^2(k) + e_{14}^2(k))} \quad (58)$$

The MSE expressions in the Cartesian (MSE_C) and joint (MSE_J) spaces for SPIDER4 are denoted as follows:

$$MSE_C = \frac{1}{N} \sum_{k=1}^N (|e_{xn}(k)| + |e_{yn}(k)| + |e_{zn}(k)|) \quad (59)$$

$$MSE_J = \frac{1}{N} \sum_{k=1}^N (|e_{11}(k)| + |e_{12}(k)| + |e_{13}(k)| + |e_{14}(k)|) \quad (60)$$

where e_{xn} , e_{yn} , and e_{zn} denote the Cartesian position tracking errors of the traveling plate along x , y , and z axes, respectively, whereas e_{11} , e_{12} , e_{13} , and e_{14} are the corresponding tracking errors in the joint space, and N is the total number of samples of the entire trajectory.

E. Obtained experimental results for case study 1

The obtained results of this case study are shown in Fig. 9, where the curves represent the tracking errors in the joint space of the three control schemes. We infer from the figure that our control proposal outperforms the PID and PID FF controllers in terms of the smaller tracking errors. We confirm this observation using the RMSE and MSE formulas, whose results are summarized in Table III. Using these data, we can calculate that for this case study, the proposed control scheme obtained improvements over the PID and PID FF control of 18.48% and 7.5%, respectively, using the RMSE formula. The corresponding obtained improvements using the MSE formula are 12.85% and 6.4%.

Considering these results, we perform the experiments of the second case study. Owing to the good performance of our control scheme compared with those of the two previous controllers, we herein compare our proposed controller to other variants of the RISE control schemes (RISE and RISE FF). Moreover, the second case study presents different scenarios where the forward speed is increased.

F. Obtained experimental results for case study 2

The obtained results for the three controllers when the desired trajectory is executed at a low speed are shown in Figs.

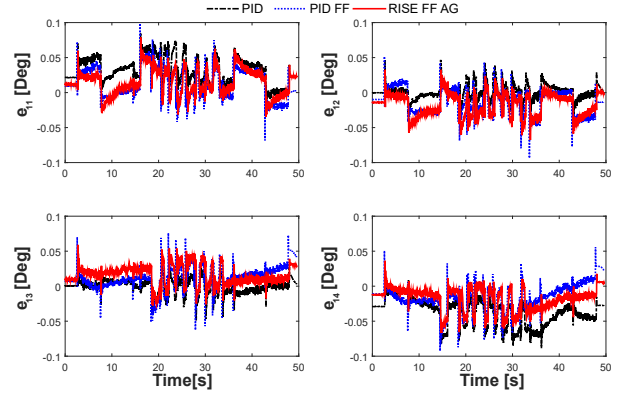


Fig. 9. Evolution of tracking errors versus time in joint space of case study 1.

8–12. Fig. 10 shows the comparison of the tracking errors in the joint space, from which we observe that the execution takes approximately 154 s when $F = 1200 \text{ mm/min}$. It can also be seen in all graphs that the tracking errors of the standard RISE controller are the worst. The tracking errors of the RISE FF and RISE FF AG controllers on motors 2 and 3 present relatively similar behavior. However, in the graph of motor 4, it can be seen that the tracking error of the RISE FF AG control is noticeably better than those of the other controllers. The variations observed in the behavior of the tracking errors of each motor may be due to the fact that although the dynamic parameters of each set of links are considered the same, in reality, they are different. To confirm our observations, we utilize of Fig. 11, which is a zoom of the graphs shown in Fig. 10 in the interval between 75 and 80 s. The evolution of adaptive gains $\mathbf{K}_s(t)$ and $\Lambda_2(t)$ with respect to time are displayed in Figs. 12 and 13, respectively. In the graphs of Fig. 12, it can be seen that the minimum value of $\mathbf{K}_s(t)$ is 33, as is established for \mathbf{K}_2 ; similarly, in Fig. 13, we observe that the minimum value taken by $\Lambda_2(t)$ is as established in matrix \mathbf{K}_3 . In addition, it can be seen from these figures that owing to this execution speed, $\mathbf{K}_s(t)$ can reach values of up to 36, whereas $\Lambda_2(t)$ can reach 4. The torques generated by the proposed RISE FF AG controller are depicted in the graphs of Fig. 14. It can be seen from the graphs of motors 1 and 2 that their values range from 100 to 270 Nm, whereas for motors 3 and 4, their values are varying between -100 and -350 Nm. This behavior is due to the horizontal orientation of the robot kinematic chains, where the acceleration of gravity affects the lower linkages (kinematic chains 1 and 2) differently than the upper linkages (kinematic chains 3 and 4). From the results shown in Figs. 10 and 11, we can conclude that our proposed control scheme outperforms the other two schemes under this operating condition with a low forward speed. However, we must utilize the criteria of the RMSEs in (57) and (58) to confirm the observations from these figures. The results of the RMSEs in the Cartesian and joint spaces are summarized in Tables IV and V, respectively. Based on the RMSEs provided in Tables IV and V, we can compute the improvement in the proposed RISE FF AG controller with respect to the two other approaches. These

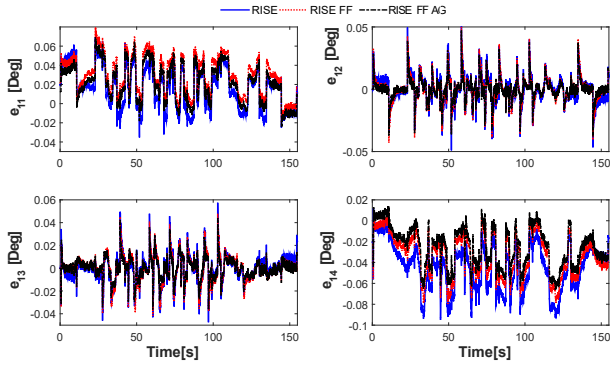


Fig. 10. Evolution of tracking errors versus time in joint space at low forward speed.

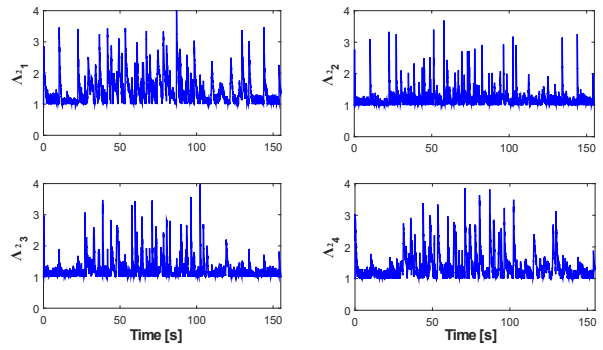


Fig. 13. Evolution of Λ_2 gains versus time at low forward speed.

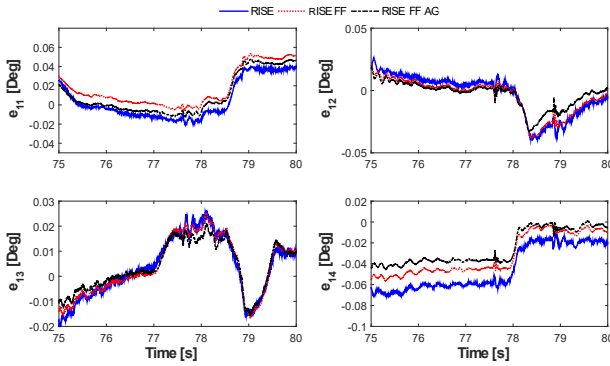


Fig. 11. Zoomed views of evolution of tracking errors versus time in joint space at low forward speed.

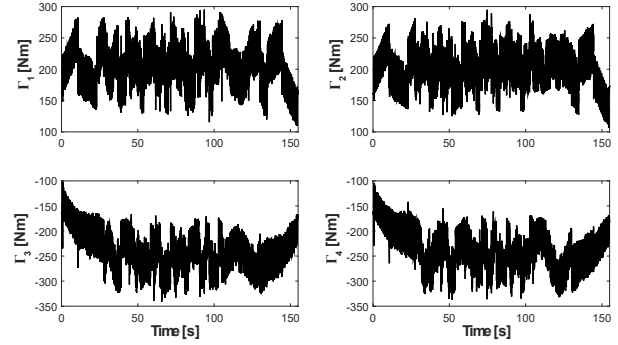


Fig. 14. Evolution versus time of control inputs generated by proposed RISE FF AG controller at low forward speed.

improvements are summarized in Table VI. Based on these results, we note that the RISE FF AG controller outperforms the standard RISE controller by 24% in the joint space and by 19% in the Cartesian space. Moreover, our control solution outperforms the RISE FF controller by 17% and 15% in the joint and Cartesian space, respectively. Considering these results, we notice a significant enhancement in the system performance when RISE FF AG is used. The piece resulting from this machining experiment using the proposed RISE FF AG controller is shown in Fig. 25a. A demonstration video is available at: <https://youtu.be/t1HaWEBy6LY>

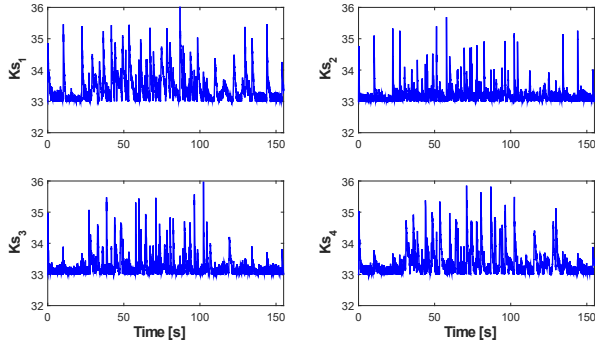


Fig. 12. Evolution of K_s gains versus time at low forward speed.

2) *Results at medium-speed:* By increasing the forward machining speed from 1200 to 2400 mm/min , the following results are obtained. At this medium speed, SPIDER4 completes the task in approximately 69 s. We note from the graphs of Fig. 15 that the joint tracking errors of the three control schemes increase with respect to the low-speed scenario. Despite this, the tracking error signals resulting from the proposed RISE FF AG controller are the closest to zero, followed by those resulting from the RISE FF controller. In addition, the performance of the standard RISE controller is the worst, presenting noticeable overshoots compared to the previous two controllers. We present zoom parts the curves of Fig. 15 in the interval between 35 and 40 in Fig. 16. From this figure, it is noticeable that the behavior of each tracking error signal confirms the above. The increase in the speed also slightly modifies the behavior of adaptive gains $K_s(t)$ and $\Lambda_2(t)$, as can be seen from Figs. 17 and 18. Furthermore, it can be seen that in some portions of the trajectory, $K_s(t)$ manages to reach values close to 37, whereas $\Lambda_2(t)$ manages to reach peak values up to 5. In addition, we can see in Fig. 19 that this speed change also increases the output torque of the motors. We notice from Fig. 19 that the torque values for motors 1 and 2 oscillate between 100 to 400 Nm , whereas those of motors 3 and 4 oscillate between -100 and -400 Nm . Similar to the task at low speed, in this case, we use the RMSE formula to quantify the tracking performance of the controllers at medium speed. The obtained results are

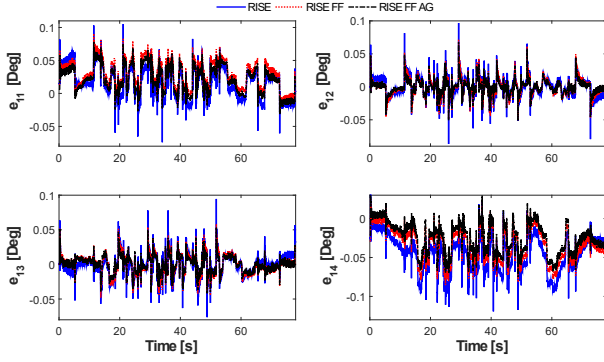


Fig. 15. Evolution versus time of tracking errors in joint space at medium forward speed.

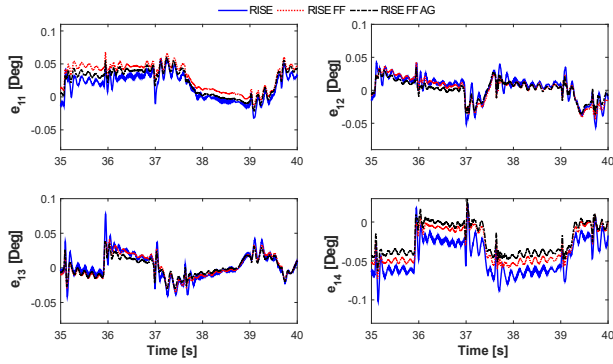


Fig. 16. Zoomed view of evolution versus time of tracking errors in joint space at medium forward speed.

listed in the third column of Tables IV and V. Based on these data, we calculate the enhancements achieved by the proposed RISE FF AG controller with respect to the two other controllers. Based on Table VI, we observe that our proposed controller has 21% and 25% improvements of in RMSEs for the Cartesian and joint space motions, respectively, whereas the improvements obtained by the RISE FF controller are 16% and 18%, respectively. The obtained piece using the RISE FF AG controller is shown in Fig. 25b, which presents that the machining quality is decreased compared to that of the previous case. This can be explained by the cutting spindle speed not increasing as the forward speed, and also by the soft nature of the machined material.

3) *Results at high speed:* The objective of conducting this experiment at speed $F = 24000 \text{ mm/min}$ is to determine the deterioration of the performance of each controller. It should be mentioned here that this speed is inadequate to perform machining tasks with materials more rigid than styrofoam because the cutting tool can be broken easily. In the following, we discuss the obtained results. The graphs of the tracking errors are depicted in Fig. 20, which show that under these conditions, the performance of the standard RISE controller is significantly degraded, whereas those of the RISE FF and RISE FF AG controllers are similar. Fig. 21 shows zoomed views of the graphs of Fig. 20 between 6 and 8 s. This figure suggests that the performance of the proposed RISE FF AG controller is slightly better than that of the RISE FF controller.

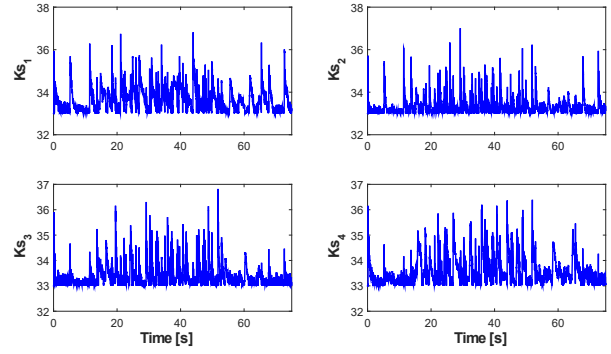


Fig. 17. Evolution versus time of K_s gains at medium forward speed.

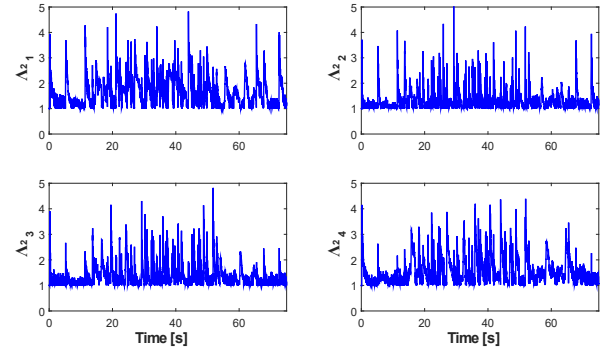


Fig. 18. Evolution versus time of Λ_2 gains at medium forward speed.

Figs. 22 and 23 shows that the values of adaptive gains $K_s(t)$ and $\Lambda_2(t)$ continue to increase with the forward speed. $K_s(t)$ manages to reach a peak values of 44, whereas $\Lambda_2(t)$ exceeds 10. Despite this behavior on the adaptive gains, it is insufficient to further reduce the tracking errors. Therefore, this execution represents the breaking point of our control proposal. The produced torques also increase, as can be seen in Fig. 24. The torque values for motors 1 and 2 range from -200 to 600 Nm, whereas those of motors 3 and 4 evolve within the range of -600 to 20 Nm. Similar to the previous scenarios, the RMSEs obtained in this experiment were registered and are summarized in Tables IV and V. In Table VI, we infer

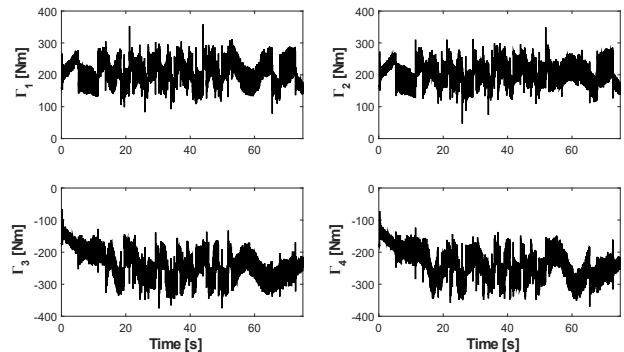


Fig. 19. Evolution versus time of control inputs generated by proposed RISE FF AG controller at medium forward speed.

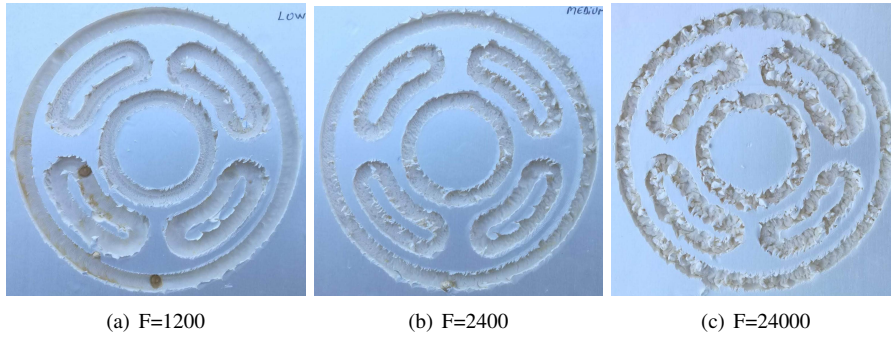


Fig. 25. View of the machining results using the proposed RISE FF AG controller with different Forward speeds (low, medium and high respectively).

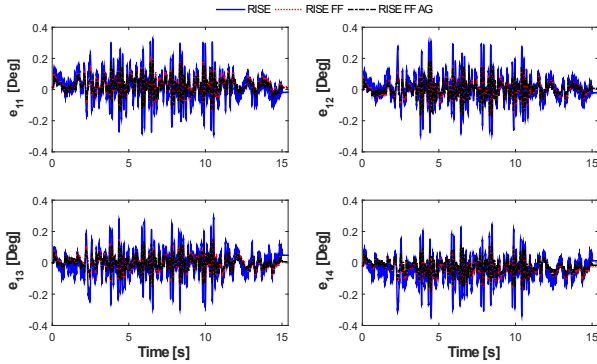


Fig. 20. Evolution versus time of tracking errors in joint space at high forward speed.

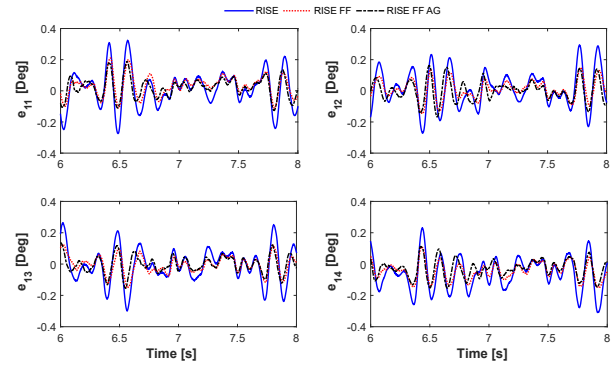


Fig. 21. Zoomed views of evolution of tracking errors in joint space at high forward speed.

that the RISE FF AG controller outperforms the standard RISE controller by 45% and 43% in the joint and Cartesian spaces, respectively, whereas the corresponding improvements relative to the RISE FF controller are only of 4% and 1.47%. These results imply that at high speeds, the performance of the proposed RISE FF AG controller is practically equivalent to that of the RISE FF controller. The same tables show that the MSEs have similar relationships as RMSEs. The resulting piece is shown in Fig. 25c, where the final result is not good owing to the excessive forward speed and the soft nature of the machined material.

It is worth mentioning that the tuning of the gains is performed at the low speed defined in the experiments. Subsequently, the obtained gains are kept unchanged for the other experimental scenarios with medium and high forward speeds to demonstrate the robustness of the proposed control scheme. Indeed, based on the graphs at low speed, the performance of the RISE controller does not differ much from those of the other two controllers, even if it is the one with the lowest performance. However, as the speed increases, the performance of the other two control schemes is less affected by the presence of more control actions. As demonstrated by the obtained real-time experimental results, our controller offers robustness towards forward speed variations as well as unexpected uncertainties, including friction effects and unmodelled dynamics.

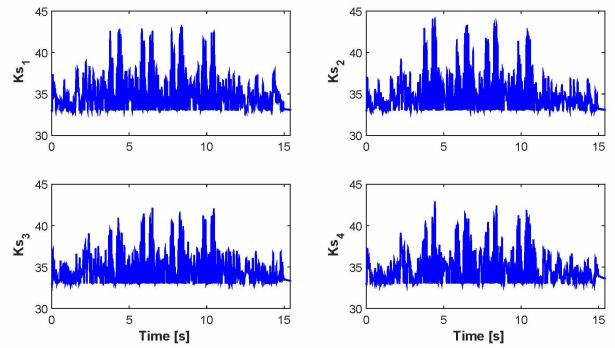


Fig. 22. Evolution versus time of K_s gains at high forward speed.

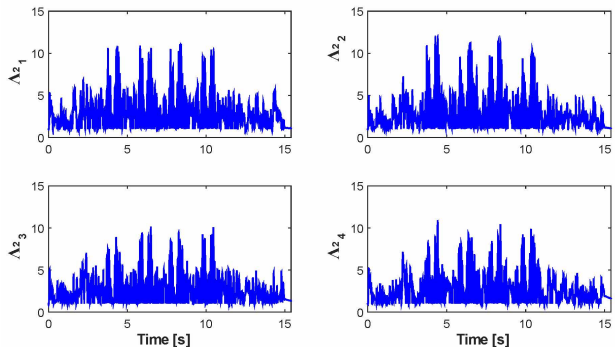


Fig. 23. Evolution versus time of Λ_2 gains at high forward speed.

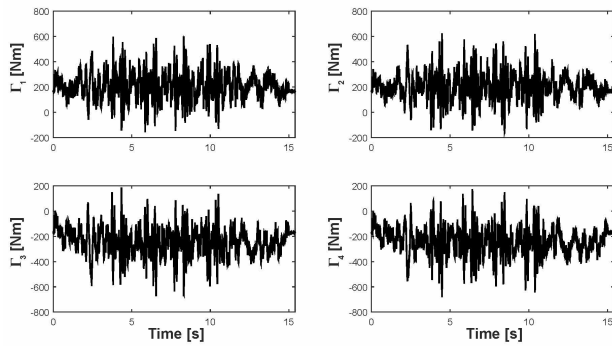


Fig. 24. Evolution versus time of control inputs generated by proposed RISE FF AG controller at high forward speed.

TABLE IV
CONTROLLERS PERFORMANCE EVALUATION USING RMSE AND MSE
CRITERIA FOR JOINT SPACE TRACKING ERRORS (DEG).

Controller	Forward speed (F)		
	1200 mm/min	2400 mm/min	24000 mm/min
RMSE			
RISE	0.0592	0.0618	0.1796
RISE FF	0.0546	0.0566	0.1051
RISE FF AG	0.0449	0.0461	0.1007
MSE			
RISE	0.0826	0.0889	0.2598
RISE FF	0.0773	0.0827	0.1714
RISE FF AG	0.0606	0.0645	0.1612

V. CONCLUSIONS AND FUTURE STUDIES

In this paper, we proposed a new adaptive extension of the RISE feedforward control. The proposed control solution aims at improving the trajectory tracking performance of PKMs for high-precision tasks, such as machining. The proposed control scheme was tested on the RA-PKM, SPIDER4, designed to perform machining operations, such as milling or drilling. Before introducing the main contribution of the paper, we briefly described the IKM and IDM of the delta-like positioning device of the SPIDER4 robot. Before to conducting the machining case study, the proposed control solution was validated against a PID controller and a PID feedforward controller.

TABLE V
CONTROLLERS PERFORMANCE EVALUATION USING RMSE AND MSE
CRITERIA FOR CARTESIAN SPACE TRACKING ERRORS (CM).

Controller	Forward speed (F)		
	1200 mm/min	2400 mm/min	24000 mm/min
RMSE			
RISE	0.0383	0.0405	0.1425
RISE FF	0.0367	0.0380	0.0794
RISE FF AG	0.0309	0.0319	0.0782
MSE			
RISE	0.0534	0.0582	0.2061
RISE FF	0.0519	0.0555	0.1294
RISE FF AG	0.0417	0.0446	0.1242

TABLE VI
ENHANCEMENT IN PROPOSED RISE FF AG W.R.T STANDARD RISE AND RISE FF USING RMSE AND MSE FOR TRACKING ERRORS IN CARTESIAN AND JOINT SPACES.

Forward speed	Cartesian Space		Joint Space	
	RISE	RISE FF	RISE	RISE FF
RMSE				
Low	19.27 %	15.73 %	24.155 %	17.75 %
Medium	21.36 %	16.06 %	25.40 %	18.55 %
High	45.12 %	1.47 %	43.93 %	4.18 %
MSE				
Low	21.91 %	19.66 %	26.59 %	21.55 %
Medium	23.32 %	19.63 %	27.51 %	22.51 %
High	39.73 %	4.01 %	34.03 %	6.34 %

For case study 2, we proposed a milling process conducted at three forward speeds (low, medium, and high) on styrofoam blocks to validate the effectiveness of the proposed control scheme. The performance of the proposed control scheme was evaluated with respect to those of the RISE feedforward and standard RISE controllers. The obtained results showed 19%, 21% and 45% improvements in the RMSEs at low, medium, and high speeds, respectively, with respect to the standard RISE controller results in the Cartesian space. Compared to the RISE feedforward controller, there were 15%, 16%, and 1.5% improvements in the RMSE at low, medium, and high speeds, respectively, in the Cartesian space. Additionally to the RMSE, we used the MSE formula to verify the effectiveness of our control solution. We inferred from Tables IV, V, and VI that the MSEs has similar percentages to the RMSEs. Before sending the control signals to the actuators, a null space operator based on the pseudo inverse Jacobian matrix was used to remove antagonistic internal forces. As a future direction, we can investigate the effect of such null-space projection operator as a potential further improvement.

ACKNOWLEDGMENTS

This study was sponsored by the French government research program, Investissements d'avenir through the Robotex Equipment of Excellence (ANR-10-EQPX-44). The first author was supported by The Mexican Council of Science and Technology (CONACYT); Award no. 593804.

REFERENCES

- [1] M. Weck and D. Staimer, "Parallel kinematic machine tools—current state and future potentials," *CIRP Annals*, vol. 51, no. 2, pp. 671–683, 2002.
- [2] A. Chemori, "Control of complex robotic systems: Challenges, design and experiments," in *2017 22nd International Conference on Methods and Models in Automation and Robotics (MMAR)*. IEEE, 2017, pp. 622–631.
- [3] T. Hufnagel and A. Müller, "A projection method for the elimination of contradicting decentralized control forces in redundantly actuated pkm," *IEEE Transactions on Robotics*, vol. 28, no. 3, pp. 723–728, 2012.
- [4] A. Müller, "Consequences of geometric imperfections for the control of redundantly actuated parallel manipulators," *IEEE Transactions on Robotics*, vol. 26, no. 1, pp. 21–31, 2009.
- [5] G. Sartori Natal, A. Chemori, and F. Pierrot, "Dual-space control of extremely fast parallel manipulators: Payload changes and the 100G experiment," *IEEE Transactions on Control Systems Technology*, vol. 23, no. 4, pp. 1520–1535, 2015.

- [6] L. R. Douat, I. Queindec, G. Garcia, M. Michelin, F. Pierrot, and S. Tarbouriech, "Identification and vibration attenuation for the parallel robot par2," *IEEE Transactions on Control Systems Technology*, vol. 22, no. 1, pp. 190–200, 2013.
- [7] J.-P. Merlet, *Parallel robots*. Springer Science & Business Media, 2006, vol. 128.
- [8] D. Zhang, *Parallel robotic machine tools*. Springer Science & Business Media, 2009.
- [9] H. D. Taghirad, *Parallel robots: mechanics and control*. CRC press, 2013.
- [10] P. C. Sheldon, "Six axis machine tool," Feb. 14 1995, uS Patent 5,388,935.
- [11] K.-E. Neumann, "Robot," Mar. 22 1988, uS Patent 4,732,525.
- [12] C. M. Clinton, G. Zhang, and A. J. Wavering, "Stiffness modeling of a Stewart platform based milling machine," Tech. Rep., 1997.
- [13] T. Toyama, Y. Yamakawa, and H. Suzuki, "Machine tool having parallel structure," Feb. 10 1998, uS Patent 5,715,729.
- [14] L. A. Castañeda, A. Luviano-Juárez, and I. Chairez, "Robust trajectory tracking of a delta robot through adaptive active disturbance rejection control," *IEEE Transactions on control systems technology*, vol. 23, no. 4, pp. 1387–1398, 2014.
- [15] M. Bennehar, A. Chemori, F. Pierrot, and V. Creuze, "Extended model-based feedforward compensation in H adaptive control for mechanical manipulators: Design and experiments," *Frontiers in Robotics and AI*, vol. 2, p. 32, 2015.
- [16] H. Saied, A. Chemori, M. Michelin, M. El-Rafei, C. Francis, and F. Pierrot, "A redundant parallel robotic machining tool: Design, control and real-time experiments," in *New Developments and Advances in Robot Control*. Springer, 2019, pp. 39–79.
- [17] M. Bennehar, G. El-Ghazaly, A. Chemori, and F. Pierrot, "A novel adaptive terminal sliding mode control for parallel manipulators: Design and real-time experiments," in *2017 IEEE International Conference on Robotics and Automation (ICRA)*. IEEE, 2017, pp. 6086–6092.
- [18] M. Bennehar, A. Chemori, and F. Pierrot, "A new revised desired compensation adaptive control for enhanced tracking: application to r-pkms," *Advanced Robotics*, vol. 30, no. 17-18, pp. 1199–1214, 2016.
- [19] M. Bennehar, A. Chemori, M. Bouri, L. F. Jenni, and F. Pierrot, "A new rise-based adaptive control of pkms: design, stability analysis and experiments," *International Journal of Control*, vol. 91, no. 3, pp. 593–607, 2018.
- [20] H. Saied, A. Chemori, M. Bouri, M. El Rafei, C. Francis, and F. Pierrot, "A new time-varying feedback rise control for second-order nonlinear mimo systems: theory and experiments," *International Journal of Control*, pp. 1–14, 2019.
- [21] J. M. Escorcía-Hernández, H. Aguilar-Sierra, O. Aguilar-Mejía, A. Chemori, and J. H. Arroyo-Núñez, "A new adaptive rise feedforward approach based on associative memory neural networks for the control of pkms," *Journal of Intelligent & Robotic Systems*, pp. 1–21, 2020.
- [22] J. M. Escorcía-Hernández, A. Chemori, H. Aguilar-Sierra, and J. A. Monroy-Anieva, "A new solution for machining with ra-pkms: Modelling, control and experiments," *Mechanism and Machine Theory*, vol. 150, p. 103864, 2020.
- [23] D. Corbel, M. Gouttefarde, O. Company, and F. Pierrot, "Towards 100G with PKM. is actuation redundancy a good solution for pick-and-place?" in *2010 IEEE International Conference on Robotics and Automation*, May 2010, pp. 4675–4682.
- [24] F. Pierrot, P. Dauchez, and A. Fournier, "Fast parallel robots," *Journal of Robotic Systems*, vol. 8, no. 6, pp. 829–840, 1991.
- [25] S. Staicu, *Dynamics of Parallel Robots*. Springer, 2019.
- [26] V. Nabat, "Robots parallèles à nacelle articulée: Du concept à la solution industrielle pour le pick-and-place," Ph.D. dissertation, Montpellier 2, 2007.
- [27] J. M. Escorcía-Hernández, H. Aguilar-Sierra, O. Aguilar-Mejía, A. Chemori, and J. H. Arroyo-Núñez, "An intelligent compensation through b-spline neural network for a delta parallel robot," in *2019 6th International Conference on Control, Decision and Information Technologies (CoDIT)*. IEEE, 2019, pp. 361–366.
- [28] R. Kouki, A. Chemori, and F. Bouani, "A new fast NMPC scheme for parallel kinematic manipulators: Design and real-time experiments," in *IEEE International Conference on Signal, Control and Communication (SCC)*, 2019.
- [29] R. Kelly, V. Santibanez, and A. Loria, *Control of robot manipulators in joint space*. Springer, 2006.
- [30] B. Xian, D. M. Dawson, M. S. de Queiroz, and J. Chen, "A continuous asymptotic tracking control strategy for uncertain nonlinear systems," *IEEE Transactions on Automatic Control*, vol. 49, no. 7, pp. 1206–1211, 2004.
- [31] P. M. Patre, W. MacKunis, C. Makkar, and W. E. Dixon, "Asymptotic tracking for systems with structured and unstructured uncertainties," in *Proceedings of the 45th IEEE Conference on Decision and Control*. IEEE, 2006, pp. 441–446.
- [32] F. Plestan, Y. Shtessel, V. Bregeault, and A. Poznyak, "New methodologies for adaptive sliding mode control," *International journal of control*, vol. 83, no. 9, pp. 1907–1919, 2010.
- [33] B. Xian, M. S. De Queiroz, and D. M. Dawson, "A continuous control mechanism for uncertain nonlinear systems," in *Optimal Control, Stabilization and Nonsmooth Analysis*. Springer, 2004, pp. 251–264.
- [34] H. K. Khalil and J. W. Grizzle, *Nonlinear systems*. Prentice hall Upper Saddle River, NJ, 2002, vol. 3.
- [35] A. Müller, "On the terminology and geometric aspects of redundant parallel manipulators," *Robotica*, vol. 31, no. 1, pp. 137–147, 2013.
- [36] A. Mueller, "Robust modeling and control issues of parallel manipulators with actuation redundancy," *Recent Advances in Robust Control: Theory and Applications in Robotics and Electromechanics*, p. 207, 2011.
- [37] T. Chai and R. R. Draxler, "Root mean square error (RMSE) or mean absolute error (MAE)?—arguments against avoiding RMSE in the literature," *Geoscientific model development*, vol. 7, no. 3, pp. 1247–1250, 2014.



Jonatan Martín Escorcía-Hernández received his B.Sc. in Robotic Engineering, M.Sc. in Automation and Control, and Ph.D. in Optomechanics from the Polytechnic University of Tulancingo (UPT), Tulancingo de Bravo, Mexico in 2013, 2017, and 2020, respectively. He is currently working as a part time professor at the UPT, teaching classes in robotics engineering. His research interests include modeling, mechanical design, and nonlinear control of robotics systems.



Ahmed Chemori received the M.Sc. and Ph.D. degrees both in automatic control from the Grenoble Institute of Technology, Grenoble, France, in 2001 and 2005, respectively. He has been a Postdoctoral Fellow with the Automatic Control Laboratory, Grenoble, France, in 2006. He is currently a tenured Research Scientist in automatic control and robotics with the Montpellier Laboratory of Informatics, Robotics, and Microelectronics. His research interests include nonlinear, adaptive, and predictive control and their applications in robotics.



Hipólito Aguilar-Sierra received the B.Sc. degree in Mechatronics Engineering from UPIITA-IPN in 2009; and M.Sc. and Ph. D degrees both in Automatic Control from the CINVESTAV Zacatenco, Mexico City, Mexico, in 2011 and 2016, respectively. He is currently a Full-time professor at Faculty of Engineering from the La Salle Mexico University. His research interests include Medical robots, Rehabilitation robots, Exoskeleton robotics and Nonlinear control.